Pal and Sato *Micro and Nano Systems Letters* (2015) 3:6
DOI 10.1186/s40486-015-0012-4

Micro and Nano Systems Letters
a SpringerOpen Journal

REVIEW Open Access

A comprehensive review on convex and concave corners in silicon bulk micromachining based on anisotropic wet chemical etching

Prem Pal[1*] and Kazuo Sato[2]

Abstract

Wet anisotropic etching based silicon micromachining is an important technique to fabricate freestanding (e.g. cantilever) and fixed (e.g. cavity) structures on different orientation silicon wafers for various applications in microelectromechanical systems (MEMS). {111} planes are the slowest etch rate plane in all kinds of anisotropic etchants and therefore, a prolonged etching always leads to the appearance of {111} facets at the sidewalls of the fabricated structures. In wet anisotropic etching, undercutting occurs at the extruded corners and the curved edges of the mask patterns on the wafer surface. The rate of undercutting depends upon the type of etchant and the shape of mask edges and corners. Furthermore, the undercutting takes place at the straight edges if they do not contain {111} planes. {100} and {110} silicon wafers are most widely used in MEMS as well as microelectronics fabrication.
This paper reviews the fabrication techniques of convex corner on {100} and {110} silicon wafers using anisotropic wet chemical etching. Fabrication methods are classified mainly into two major categories: *corner compensation method* and *two-steps etching technique*. In corner compensation method, extra mask pattern is added at the corner. Due to extra geometry, etching is delayed at the convex corner and hence the technique relies on time delayed etching. The shape and size of the compensating design strongly depends on the type of etchant, etching depth and the orientation of wafer surface. In this paper, various kinds of compensating designs published so far are discussed. *Two-step etching method* is employed for the fabrication of perfect convex corners. Since the perfectly sharp convex corner is formed by the intersection of {111} planes, each step of etching defines one of the facets of convex corners. In this method, two different ways are employed to perform the etching process and therefore can be subdivided into two parts. In one case, lithography step is performed after the first step of etching, while in the second case, all lithography steps are carried out before the etching process, but local oxidation of silicon (LOCOS) process is done after the first step of etching. The pros and cons of all techniques are discussed.

Keywords: MEMS; Silicon anisotropic etching; Micromachining; Alkaline solution; TMAH; KOH; Convex and concave corners; Corner compensation

Introduction

Micromachining is the most popular technique for the formation of micro/nanostructures for microelectromechanical systems (MEMS) [1-8]. It is divided into two categories: *surface micromachining* and *bulk micromachining* as presented in Figure 1 [9,10]. In surface micromachining, the micro/nanostructures are realized by the deposition and etching of thin structural and sacrificial layers on the top of the substrate, whereas bulk micromachining defines structures by selectively etching inside a substrate such as freestanding mechanical structures (e.g. beams and membranes) or three-dimensional features (e.g. cavities/grooves, through holes, and mesas). Silicon has excellent mechanical properties, which make it a promising candidate material for micromachining and microengineering [11,12]. Bulk micromachining is further divided into two major classes: *wet bulk micromachining* and *dry bulk micromachining*. Either method can be employed for isotropic or anisotropic etching. Dry etching involves the use of gas-phase etchants in plasma [13-18]. Due to the

* Correspondence: prem@iith.ac.in
[1]Department of Physics, MEMS and Micro/Nano Systems Laboratory, Indian Institute of Technology Hyderabad, Hyderabad, India
Full list of author information is available at the end of the article

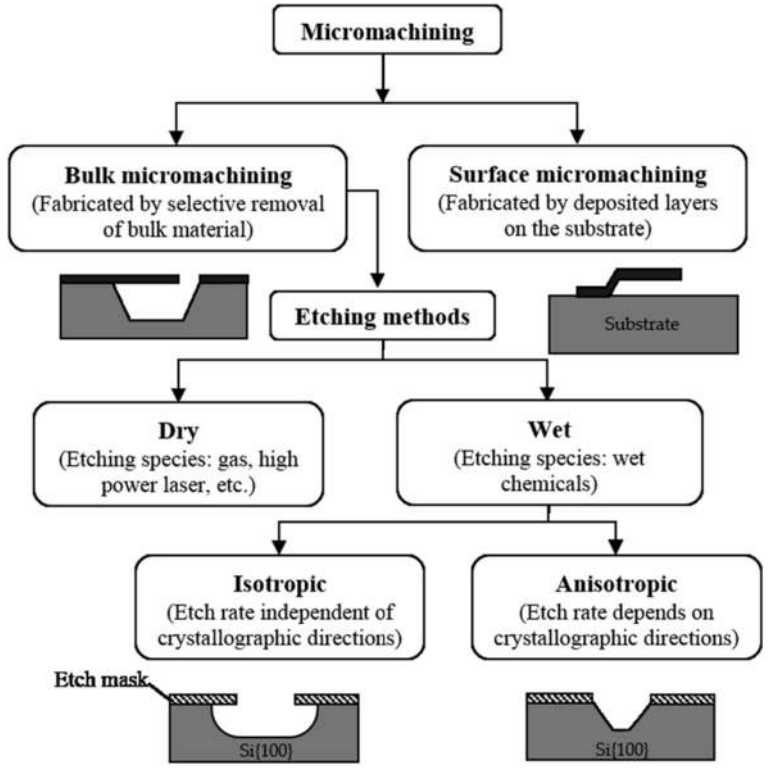

Figure 1 Classification of micromachining for the realization of micro/nanomechanical structures for MEMS/NEMS.

involvement of plasma in dry etching, it is often called plasma etching. Ion and laser beams based etchings also fall into the category of dry etching [19,20]. The dry etching process typically etches directionally and the etch rate is almost crystallographic orientation independent. On the other hand, wet etching is carried out in liquid-phase ("wet") etchants and can further be subdivided into *isotropic etching* and *anisotropic etching* as shown in Figure 1. In isotropic etching, the etch rate does not depend on the orientation of the substrate i.e. etching proceeds in all directions at equal rates. A mixture of hydrofluoric (HF), nitric (HNO_3), and acetic (CH_3COOH) acids (i.e. HNA) is most commonly used as silicon isotropic wet etchant [21,22]. In this composition, acetic acid can be replaced by water and the etch rate of silicon depends on the proportion of the acids in the mixture. In the case of wet anisotropic etching, the etch rate depends on the orientation of the crystallographic plane of the substrate. The anisotropic etchants etch materials much faster in one direction than in another, exposing the slowest etching crystal planes over time [1,2,4,10,23-27]. Several kinds of aqueous alkaline solutions such as potassium hydroxide solution (KOH) [23-26,28-35], tetramethylammonium hydroxide (TMAH) [27,36-45], ethylenediamine pyrocatechol water (EDP or EPW) [26,35,46,47], hydrazine [23,48,49], ammonium hydroxide [50], and cesium hydroxide (CsOH) [51] are employed for silicon wet anisotropic etching. Among these etchants, potassium hydroxide (KOH) and tetramethylammonium hydroxide (TMAH) are most frequently used. TMAH is a complementary metal oxide semiconductor (CMOS) compatible etchant as it does not contain alkali ions, unlike KOH. In all kinds of alkaline solutions, {111} are the slowest etching planes, while {110}, {100} and other high index planes are the fast etching planes. The etch rate and the etched surface morphology depend on several parameters of the etchant such as concentration, etching temperature, agitation during etching, additives, etc. However the selection of the type of etching process (dry or wet) mostly depends upon the requirement of the end product. Wet anisotropic etching has several advantages over dry etching including low cost, simple experimental setup, easy handling, batch processing, orientation dependent etch rate, unmatched capability to release mechanical structures, etc. Orientation dependent etch rate is employed to develop microstructures with vertical as well as slanted sidewalls. Wet anisotropic etching has been widely used in silicon based MEMS fabrication such as inkjet head [1,2], RF-MEMS components [52-55], mechanical sensors [56-61], thermal sensors [62-64], micro/nano calorimeters [65-67], microfluidic devices [68-71], and bio/chemical sensors [72-75], atomic force microscopy tips [76-78], etc.

In wet anisotropic etching, stable etched profiles are shaped by slowest etch rate planes (i.e. {111}). In the

case of Si{100} wafer, {111} planes appear at the edges aligned along <110> directions as shown in Figures 2(a) and 3(a). These planes form a square shape cavity/groove. In the case of Si{110} wafer, six {111} planes are exposed during the etching process. The intersection of {111} planes at {110} surface forms a polygon as shown in Figures 2(b) and 3(b) [1,79]. The edges of polygon structure are oriented along <112> and <110> directions. Using <112> and <110> directions, different shapes pattern can be formed. <112> direction contain vertical {111} planes, whereas <110> directions comprise slanted {111} planes. The <112> directions can be used to form a parallelogrammic structure. The intersection of {111} planes forms either a concave corners (<180 i.e. corners turning inside) or a convex corners (>180° i.e. corners turning outside). Although both types of corners are bounded by {111} planes, their etching characteristics are exactly opposite to each other. The concave corner remains intact during the etching, while convex corners are immediately attacked by the etchant leading to undercut. Hence the fabrication of structures with protected convex corner is a tedious task for both {100} and {110} silicon wafers. The mechanism of undercutting [79-87] and the fabrication of convex corners [24,88-128] are widely investigated. Although we have published a review article in 2007 on the fabrication of convex corners, it covers the techniques reported upto 2005 for Si{100} wafers only [109]. The fabrication methods of convex corners on {110} wafers were not discussed in this article. Additionally, over the past few years, different types of techniques are reported for the protection of convex corners in different kinds of etchants for both {100} and {110} silicon wafers [119-128].

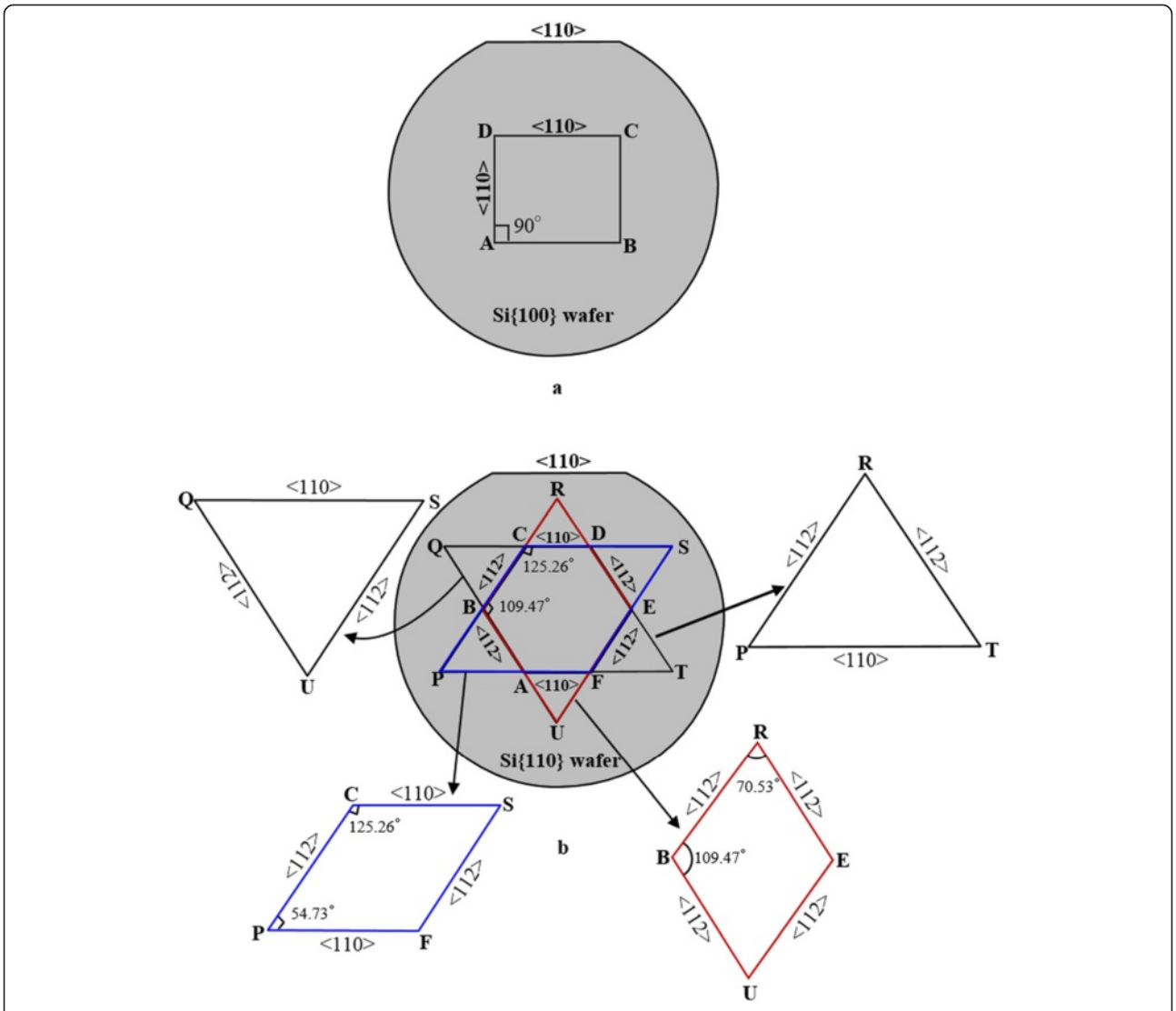

Figure 2 Schematic illustration of different shapes formed by the directions at which {111} planes appear during etching (a) <110> directions on Si{100} surface (b) <112> and <110> directions on Si{110} surface.

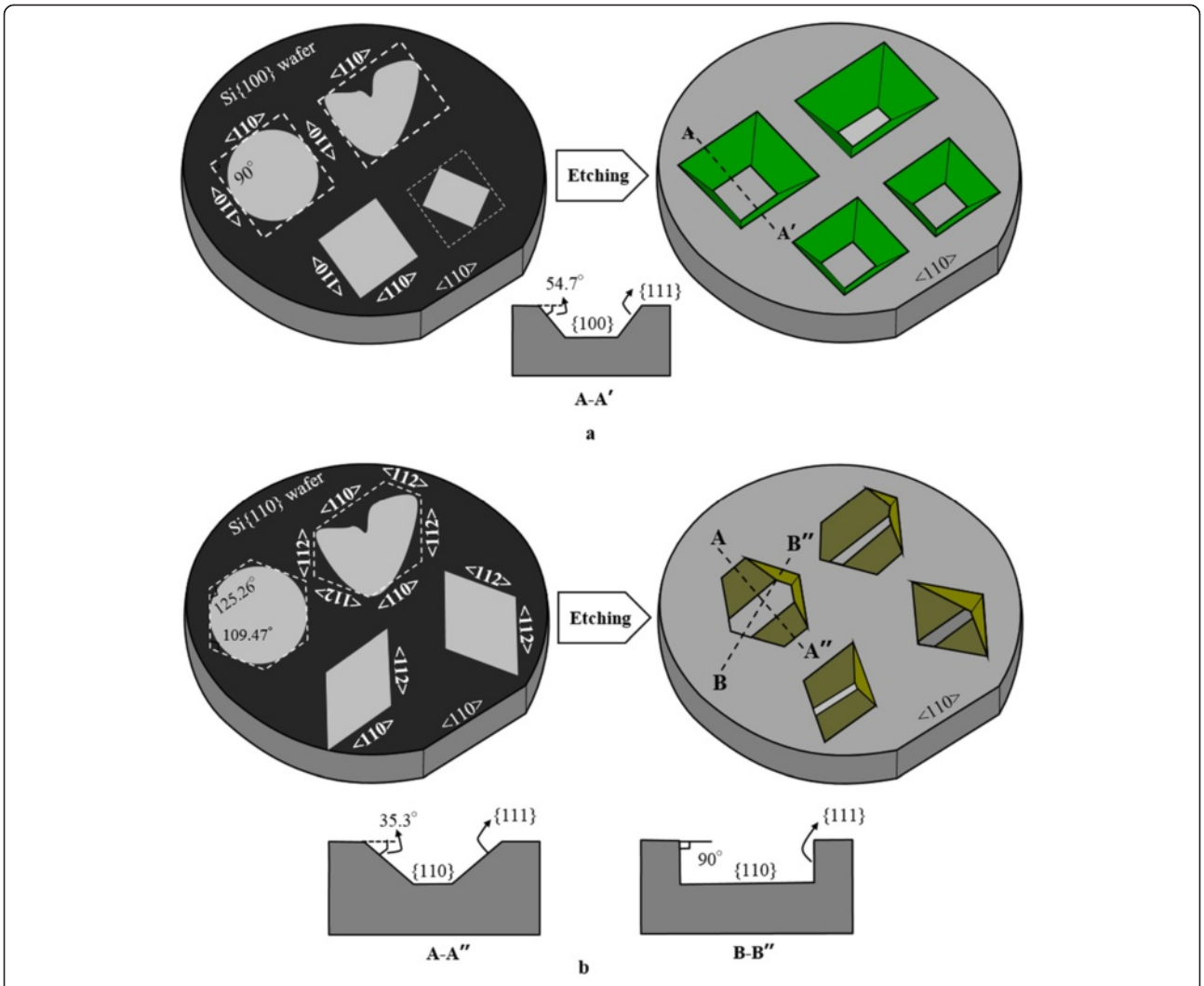

Figure 3 Schematic representation of the etched profile using different shapes mask geometries in (a) {100} and (b) {110} silicon wafers.

In this article, we have reviewed the fabrication methods of convex corners on {100} and {110} silicon wafers using silicon bulk micromachining based on anisotropic wet chemical etching. This paper is intended to be an independent guide to understand the main reason behind undercutting, protection of convex corners, the advantages and disadvantages of undercutting in silicon-based MEMS fabrication, etc. We have discussed the issues of "where to use what kinds of structure and the points to be considered to select the type of etchant".

Difference between etch rate, underetching and undercutting

In order to select an etchant for silicon wet anisotropic etching, various parameters such as etch rate, anisotropy, handling, etching selectivity over other materials (especially with masking material), CMOS compatibility, undercutting, etc. are considered. The etch rate and undercutting are primarily used to determine the etching time and the etched shape of a structure. The etch rate is a measure of the thickness removed per unit time. It is measured along the direction perpendicular to the surface being etched. Etch rate of crystallographic plane {hkl} (i.e. $R_{\{hkl\}}$) can be expressed by following relation:

$$R_{\{hkl\}} = \frac{d_{\{hkl\}}}{t} \tag{1}$$

where $d_{\{hkl\}}$ and t are the etch depth measured perpendicular to the {hkl} plane and the etching time, respectively.

The etch rate is a very useful parameter of an anisotropic etchant as it is used to estimate other parameters such as throughput, anisotropy ratio between two planes (particularly amongst {100}, {110} and {111} planes), undercutting,

etc. The absolute and relative etch rates of different crystallographic planes are usually strong function of the etchant type, concentration and etching temperature. Moreover, the etch rates are significantly affected by the impurities (or additives) in the etchant. A low concentration of IPA in KOH [33,129-133] and a very small concentration of surfactant (e.g. 0.1% v/v) in TMAH [134-147] ensure a significant reduction in the etch rates of {110} and its vicinal planes (or the planes between {110} and {111} surfaces such as {441}, {331}, {221}, etc.). Recently, surfactant added KOH is characterized to alter the etching anisotropy and etched surface morphology [148,149]. The etch rates of principle orientations (i.e. {100}, {110} and {111}) can easily be determined using {100}, {110} and {111} silicon wafers which are commonly available in the market. In order to obtain the detailed data on the crystal orientation dependence of the etch rate, either a wagon wheel structure (a series of narrow and long mask opening rotated by a small angle to each other about a center) as shown in Figure 4 [25,150-154] or a silicon hemisphere as shown in Figure 5 [29,34,37,38] is employed. Wagon wheel structure gives the etch rates of limited number of crystallographic planes, while silicon hemisphere provides etch rate data of all possible crystallographic planes as presented in Figure 5. The widest application of wagon wheel pattern is to know the relation between lateral etch rate and the crystallographic direction on different orientation surfaces (e.g. {100}, {110}). As the Si{111} planes have lowest etch rate in anisotropic wet chemical etching, the direction containing {111} planes (e.g. <110> and <112>) exhibit minimum lateral etching as presented in Figure 4.

The *undercutting* and *underetching* are the lateral etching which occur under the masking layer. Mostly, the words "undercutting" and "underetching" are used interchangeably. In reference [1], underetching is specifically used to define the etching under the mask edges which do not contain extruded/convex corners. This kinds of underetching takes place due to the misalignment of mask edges or/and owing to finite etching of the {111} planes. If the mask patterns include convex corners, the underetching at convex corners is termed as undercutting. Hereafter, mainly

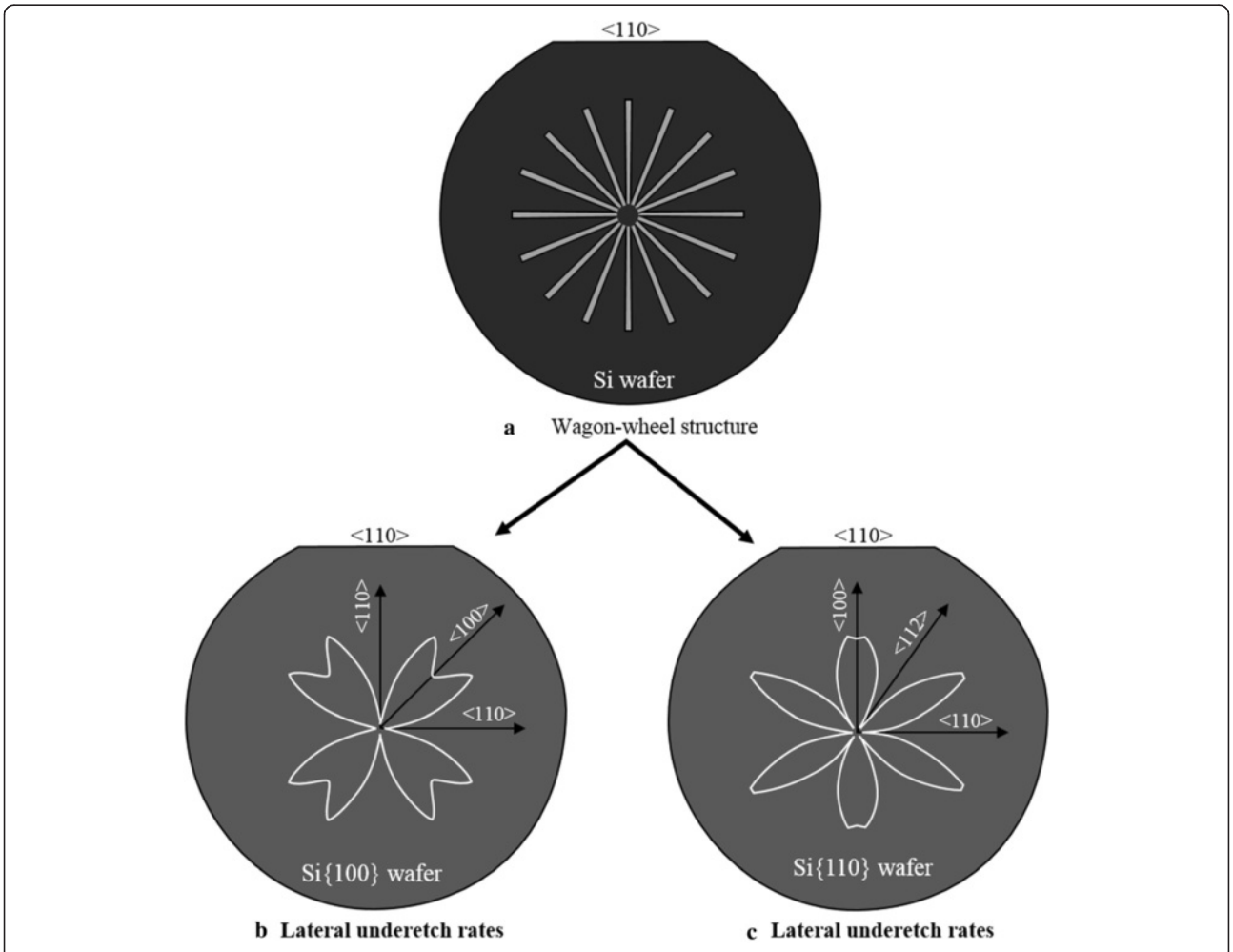

Figure 4 The diagram of lateral underetch rates as a function of orientation on silicon wafer using wagon-wheel structure (Etchant: 50% KOH at 78°C). These patterns provide relative etch rates rather than absolute etch rates.

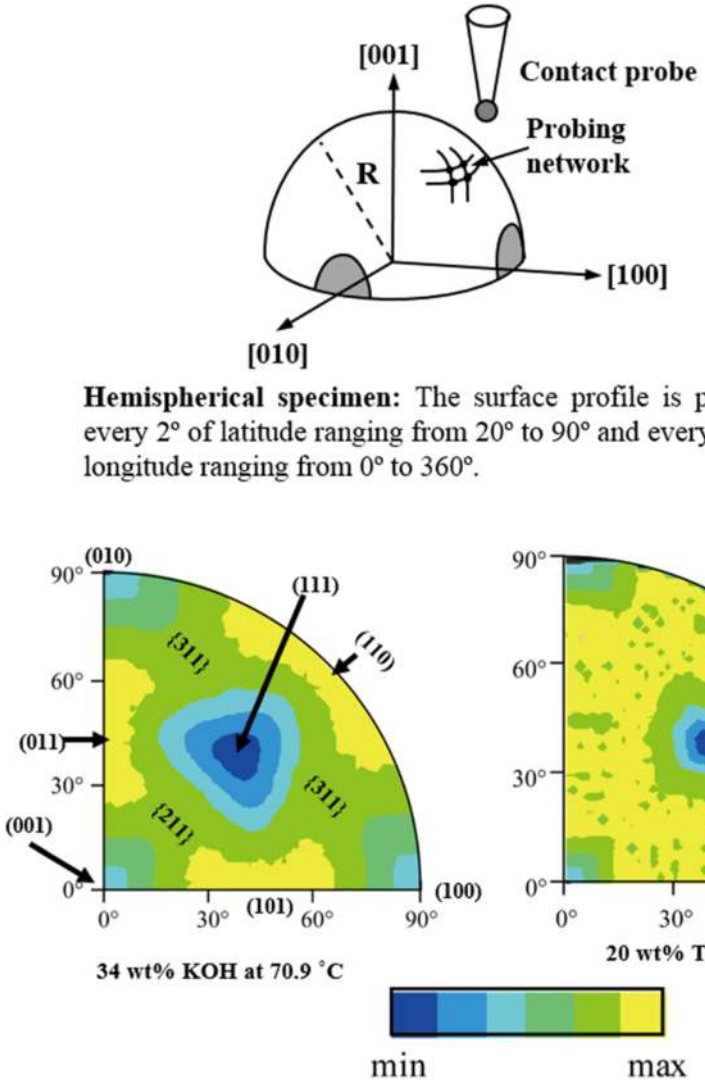

Figure 5 Comparison of the contour patterns of the etching rates in KOH and TMAH solutions obtained using silicon hemisphere [34].

undercutting word is used for the lateral etching at any type of mask edge and corner. In the case of {100} wafers, significant undercutting takes place at the edges aligned along non-<110> directions if an etchant is used without any additives (i.e. pure KOH or TMAH). In order to fabricate the square/rectangle cavity of controlled dimensions in {100} silicon wafers, the sides of square/rectangle mask opening are aligned along the <110> directions as the mask edges aligned with these directions exhibit minimum undercutting owing to the appearance of {111} planes. If the sides are slightly misaligned from the <110>direction, the undercutting starts at the edges resulting in a cavity of bigger dimensions than the requirement as shown in Figure 3.

Figure 6 illustrates the undercutting at the mask edges aligned along <100> directions. The undercutting at sharp convex corners on {100} and {110} surfaces are shown in Figures 7 and 8, respectively. In this paper, the sharp convex and concave corners are always referred to the corners bounded by only {111} planes. Due to undercutting, any arbitrary shape of mask opening on {100} wafer acquires a square shaped cavity after a sufficient time (or prolonged time) of wet etching as shown in Figure 3(a). The sidewalls of the cavity are slowest {111} planes. In the case of {110} surface, except the parallelogrammic structures formed by <112> and <110> directions, any kinds of mask opening become a polygon shape cavity after a sufficiently long etching time as illustrated in Figure 3(b). The final shape and size can be determined using etching parameters and trigonometric relations. The ratio of undercut length (l) to etch depth (d) is defined as *undercutting ratio* ($U_r = l/d$). This review article is primarily focused on the role of convex corners in silicon-based MEMS. Hence, the undercutting issue is addressed for sharp convex corners.

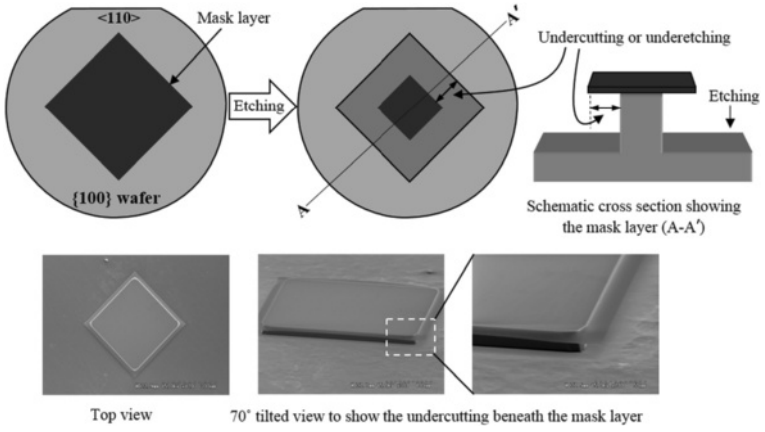

Figure 6 Schematic diagram with SEM pictures illustrating undercutting and etching.

Alignment of mask edges along crystallographic directions on wafer surface plays a significant role in controlling the shape and size of etched profiles. In order to align the mask patterns with respect to the crystallographic directions on the wafer surface, primary flat is commonly employed as reference. In this case, any degree of misorientation in primary flat leads to the misalignment of mask patterns with respect to crystallographic directions. A small degree of misalignment of the mask edge with crystallographic direction results in oversized microstructure due to the undercutting at the misaligned mask edges. Therefore, in the fabrication of silicon-based MEMS structures using wet etching, a high precision alignment of mask pattern to crystal orientation is desirable in order to control the dimensions of fabricated structures. Several studies have been performed for the precise alignment of mask patterns with respect to crystallographic directions on {110} and {100} silicon wafers [155-160]. All these techniques are based on the development of mask patterns to create the pre-etched pattern for the identification of crystallographic directions, for instance, <110> direction on {100} oriented wafer surface.

Advantages and disadvantages of corner undercutting

In the fabrication of wet bulk micromachined structures, undercutting at convex corners plays a significant role. It has its own advantages and disadvantages in fabrication process. For the realization of suspended/freestanding microstructures made of materials such as p^+-Si, SiO_2, Si_3N_4, etc., silicon beneath a structural component needs to be removed [1-5,10,70,161-163]. If the process is done only on one side of the wafer, the removal of underneath material

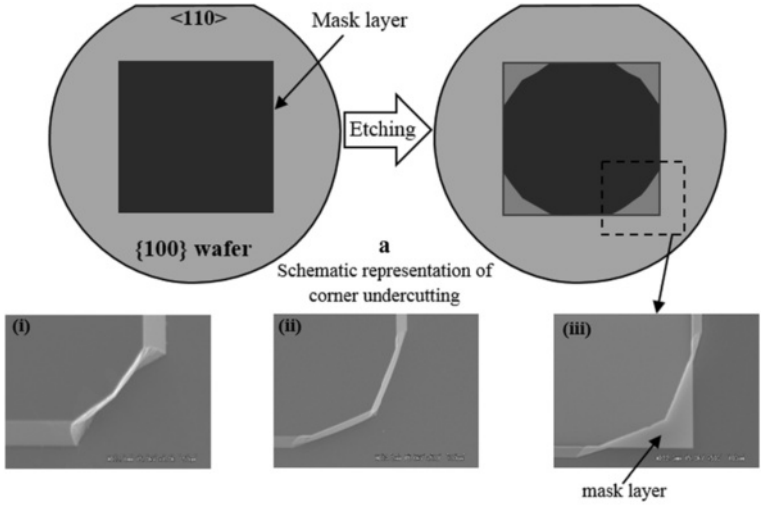

Figure 7 Undercutting at the convex corners of the mask pattern on Si{100} wafer.

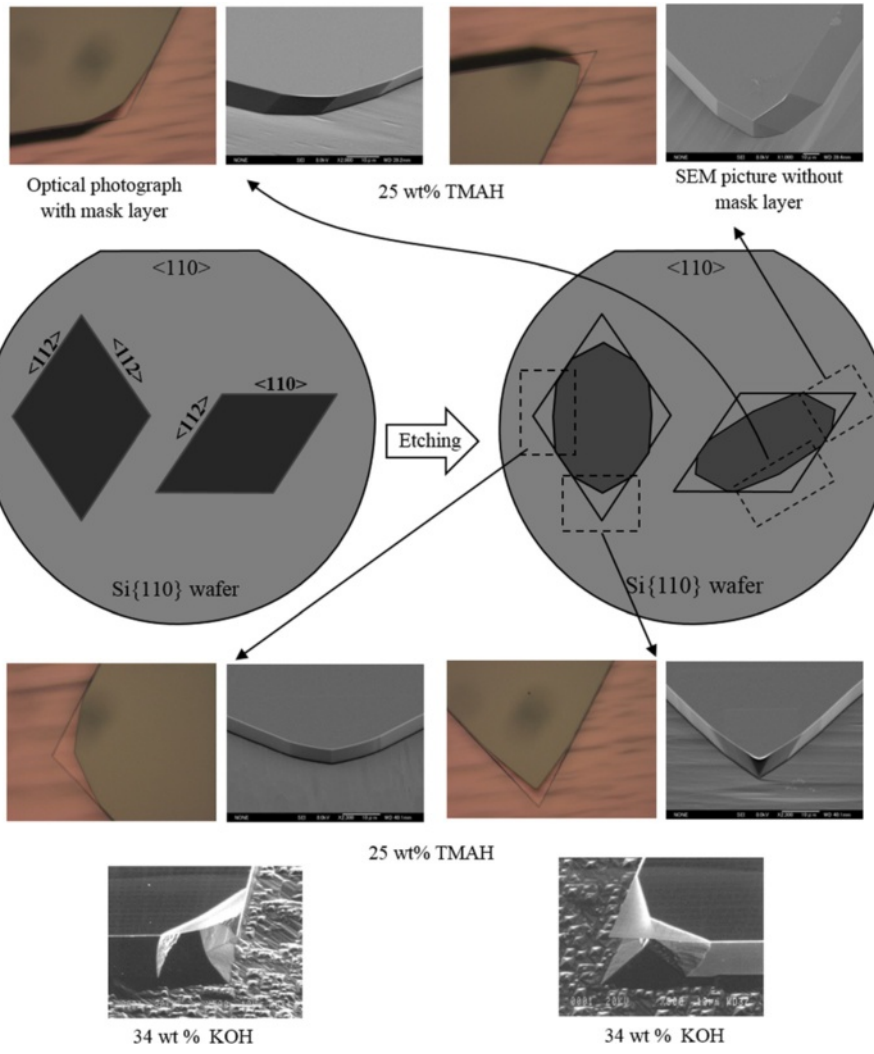

Figure 8 Undercutting at the convex corners of the mask pattern on {110} silicon wafer in 25 wt% TMAH and 34 wt% KOH [116,128].

is only possible by undercutting process [70,161,162]. In order to minimize the release time as fast as possible undercutting is desirable. Hence, a high undercutting rate is advantageous for the formation of suspended structures. Figure 9 illustrates the application of undercutting for the fabrication of suspended cantilever beam.

In many cases, undercutting is detrimental as it distorts the desired shape of the structure e.g. proof mass for accelerometer, mesa structures, chip isolation grooves, bent V-grooves, etc. as shown in Figure 10 [1,2,39,57,70,92,95,118,120]. Thus, the undercutting is unwanted for the fabrication of these types of microstructures and it is highly anticipated to eliminate this problem by some means. Considering the advantages and disadvantages of undercutting, special attention must be given while designing mask pattern. Several methods which are employed to circumvent the problem of undercutting are reviewed in this article.

Why does undercutting starts at convex corners?

The etching characteristics of KOH with different alcohol additives are presented in Figure 11 [133]. The undercutting in pure KOH is significantly high, whereas it is dramatically suppressed in alcohol-added solutions. In the case of TMAH, the surfactants are best additives to minimize the undercutting at all types of corners and edges as shown in Figure 12 [134-146]. In pure alkaline solutions, the convex corners encounter severe undercutting, while no undercutting is observed at concave corners as illustrated in Figure 9. Now the question is, why does the undercutting start at convex corner and not at the concave corner, even though both types of corners are formed by the intersection of {111} planes. Moreover, why the undercutting is suppressed when the etching is done in alcohol-added KOH (or surfactant-added TMAH) as shown in Figures 11 and 12. Several models have been developed to explain the mechanism behind the undercutting at convex

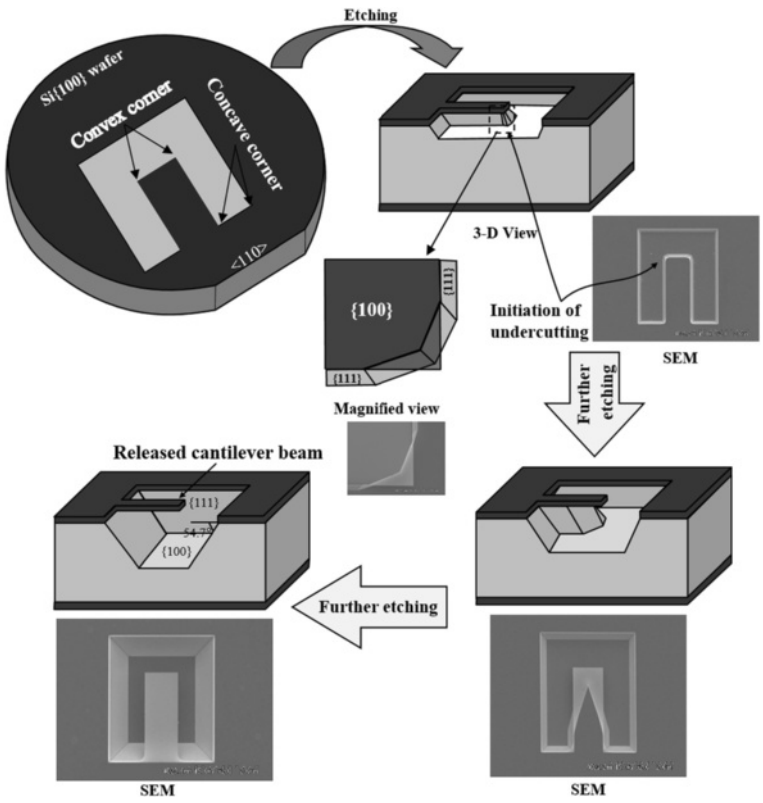

Figure 9 Schematic diagrams with SEM pictures representing the application of convex corner undercutting in the releasing of microstructure for MEMS.

corner [80-86]. Most of the models talk about Si{100} wafers as this orientation is most widely employed in microfabrication. In general, they explain that the undercutting occur due to the appearance of high etch rate planes during etching process [80-85]. At the atomistic scale, the convex corner exposes low coordination atoms with high removal rates, hence inducing the emergence of fast etching planes as the sloping facets or bevels [164]. Wei Dong *et al.* explained the undercutting mechanism on {110} surface by comparing the density of break bonds (i.e. dangling bonds) at convex corner and {111} surface [86]. The break bond density of silicon atoms at convex corner is higher than that of {111} planes. This fact results in undercutting at convex corner as the removal rate of the atoms belonging to convex corner is higher than that of the atoms pertaining to {111} planes. The silicon atoms at concave corners do not contain any break bond and therefore the shape of concave corner is not distorted.

Recently, a simple model is developed to describe the etching characteristics of concave and convex corners on {100} and {110} surfaces in all kinds of wet anisotropic etchants [79,87]. This model is based on the etching behavior of the tangent planes at the convex edge and the role of dangling bonds in etching process. There are infinite number of planes that can pass through the convex edge of the mesa structure. Although infinite number of planes can pass through this edge, the silicon atoms of the convex edge belong fully to only the tangent plane at that edge as can quite simply be noticed in Figure 13. The orientation of tangent planes depends on the angle of convex corner (i.e. acute, right and obtuse). The tangent planes at the acute and obtuse convex corners are {100} and {110}, respectively. In the case of right angled convex corner on {100} wafer, the orientation of tangent plane is {110}. In the anisotropic etchants, the etch rates of {110} and {100} planes is higher than that of the {111} planes as presented in Figure 5. Therefore, the undercutting starts at convex edge as the tangent planes containing the atoms of convex ridge exhibit much higher etch rate than that of the {111} planes which form the corners.

As presented in Figure 12, undercutting at convex corner is significantly reduced in surfactant-added TMAH. The etch rate of Si{100} is almost the same as in pure and surfactant-added 25 wt% TMAH (Figure 12(c), while the etch rates of {110} and its vicinal planes are decreased to a considerably low level when a very small amount of surfactant is added into the etchant. The main cause behind the change in etching rates is attributed to the orientation dependent adsorption of surfactant molecules during etching process. It has been confirmed through Fourier transform infrared (FTIR) and Ellipsometric studies that the maximum adsorption is for {111}

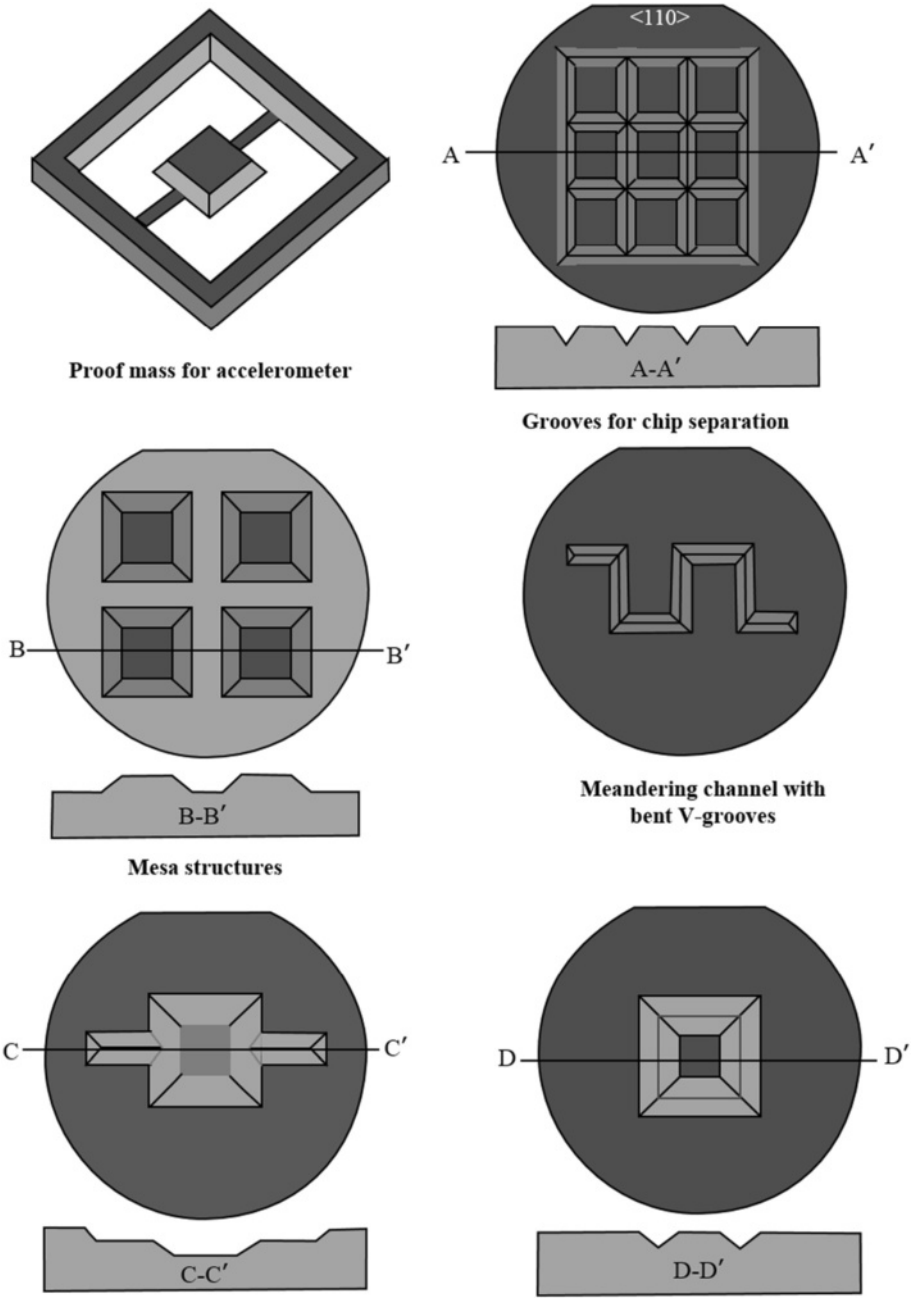

Figure 10 A few examples of the microstructures in silicon wafer where undercutting at convex corners is absolutely undesirable.

surface followed by {110} and {100} surfaces [135-137]. The etch rate of {100} is almost unaffected because the layer of surfactant molecules on {100} surface is not able to protect the surface from the etchant owing to its lower adsorptivity. In the case of Si{110}, significant reduction in the etch rate indicates that the layer of adsorbed surfactant molecules is sufficient enough to shield the surface from the etchant. Since the tangent plane at the convex corner on {100} surface is {110}, the surfactant molecules form a dense layer on the convex corners as illustrated in Figure 14. This dense layer inhibits the etchant to react chemically with the silicon atoms at the corner that results in dramatic reduction in the undercutting.

In the case of concave corner, regardless of its shape, the concave ridge consists of atoms with no dangling bonds (or unsatisfied bonds) i.e. all the bonds of concave edge atoms are engaged with neighboring atoms. Owing to this fact, no undercutting is initiated at the concave corners and they remain intact and firmly defined by the intersection of {111} planes regardless of the etching

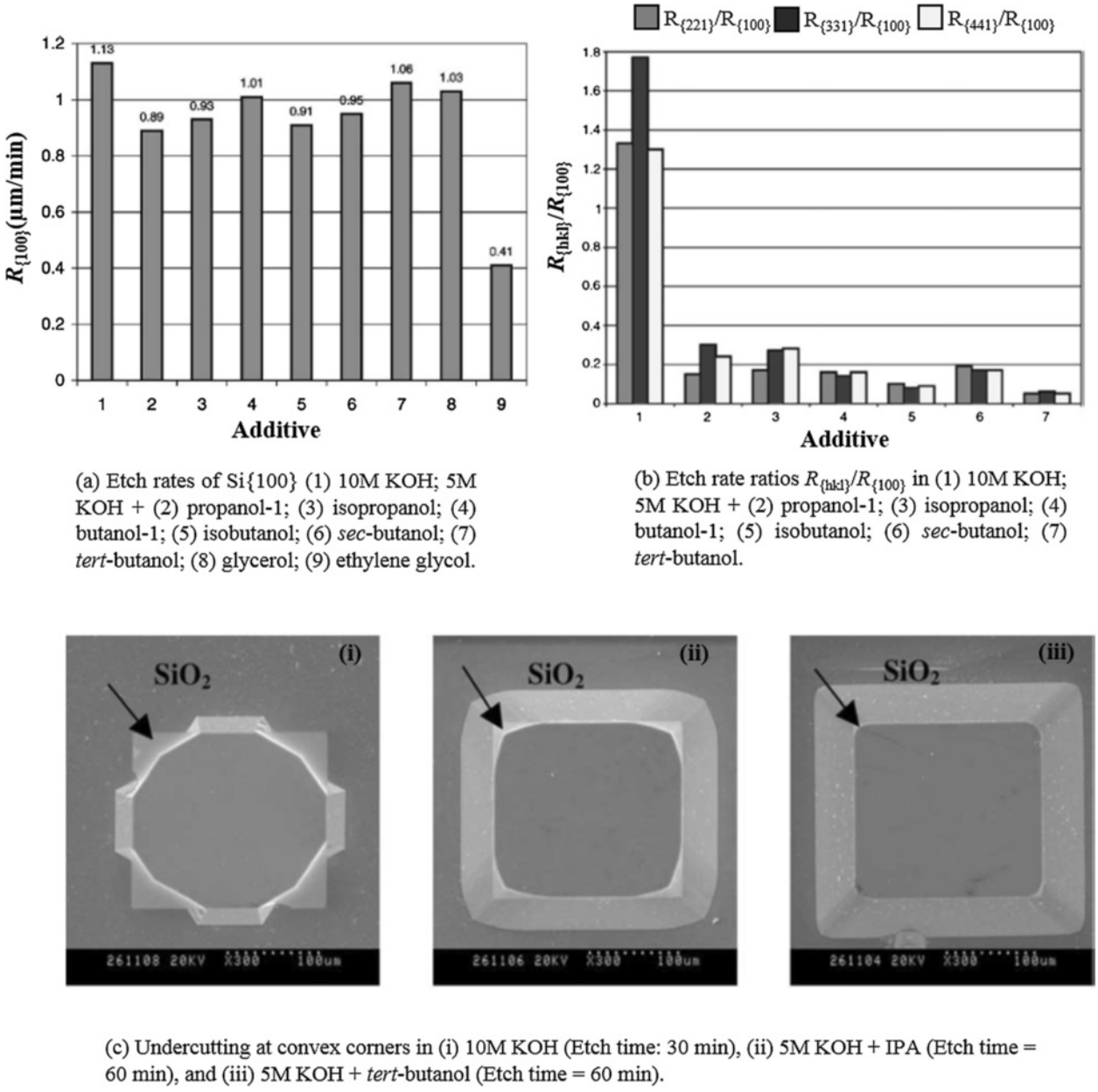

(a) Etch rates of Si{100} (1) 10M KOH; 5M KOH + (2) propanol-1; (3) isopropanol; (4) butanol-1; (5) isobutanol; (6) *sec*-butanol; (7) *tert*-butanol; (8) glycerol; (9) ethylene glycol.

(b) Etch rate ratios $R_{\{hkl\}}/R_{\{100\}}$ in (1) 10M KOH; 5M KOH + (2) propanol-1; (3) isopropanol; (4) butanol-1; (5) isobutanol; (6) *sec*-butanol; (7) *tert*-butanol.

(c) Undercutting at convex corners in (i) 10M KOH (Etch time: 30 min), (ii) 5M KOH + IPA (Etch time = 60 min), and (iii) 5M KOH + *tert*-butanol (Etch time = 60 min).

Figure 11 Etching characteristics of KOH solutions at 80°C without and with different alcohol additives [133]. With permission from Elsevier, Copyright 2002.

time, etch depth, etchant concentration and the etching temperature, as schematically shown in Figure 13.

Etched profile of undercut convex corners

The initiation of undercutting at convex corner exposes other types of high etch rate planes whose orientations depend on the type of wafer surface. The contour of etched corner is analyzed by the lateral undercutting etch rates in different directions which are estimated by the etching of a wagon wheel structure as shown in Figure 4. The lateral etch rate (or underetching) at different crystallographic directions on a plane surface depends on the type of etchant, concentration and temperature [4,25]. Consequently the amount of undercutting and the geometry of the developed etch front are typically different for different etchants. The final etch front of the undercut convex corners are constructed by the intersection of the directions which are parallel to the maximum lateral etch rate directions nearest to the edges forming convex corners as shown in Figures 15 and 16 for {100} and {110} surfaces, respectively. This leads to differently shaped etched profile at different

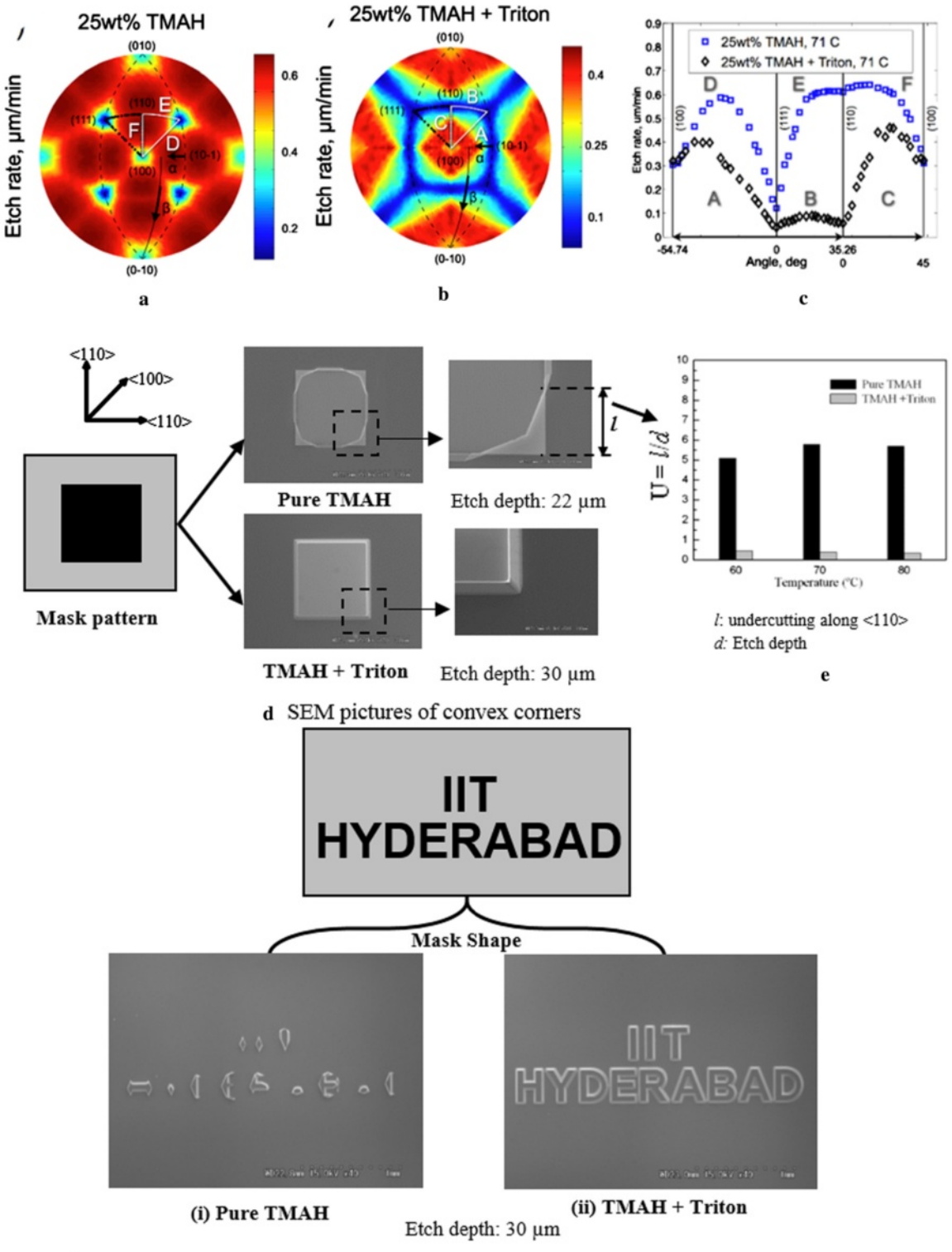

Figure 12 Etching characteristics of pure and surfactant (Triton X-100) added 25 wt% TMAH: (a)-(c) 3D distribution and 2D plot of the etch rates [38]; (d) etched profiles of the convex corners (e) undercutting ratio (*l*/d) at different temperatures (f) Micromachining of alphabet letters in Si{100} using (i) pure TMAH and (ii) TMAH + Triton.

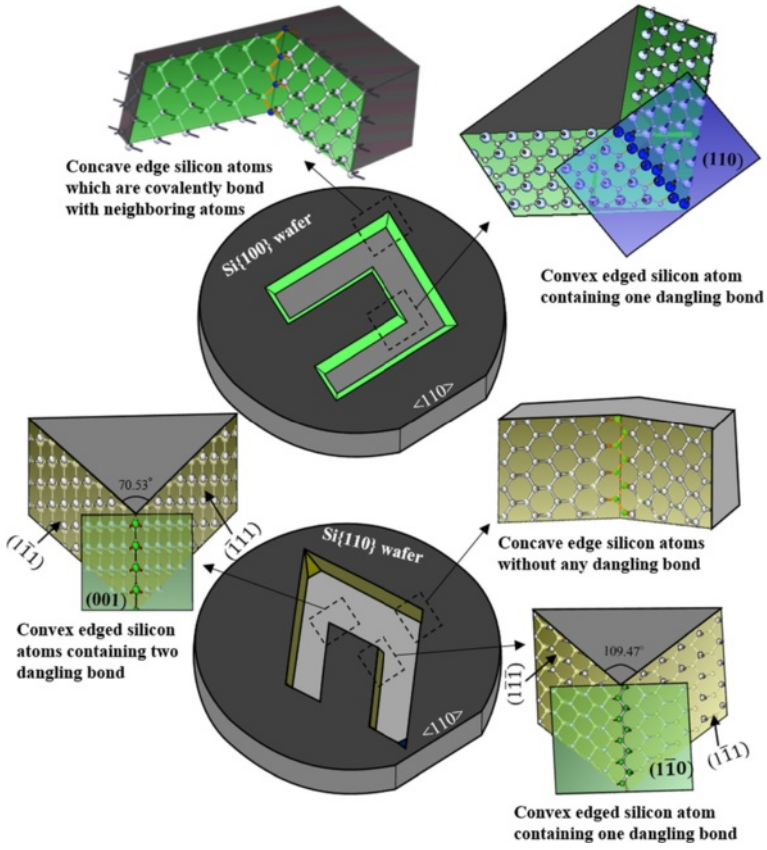

Figure 13 Schematic representation of concave and convex corners in {100} and {110} wafers. The close-up view of concave corner exhibiting silicon atoms of {111} surface with one dangling bonds, while the atoms belonging to the edge of concave corner do not contain any dangling bond. The close-up view of convex corner showing the tangent planes.

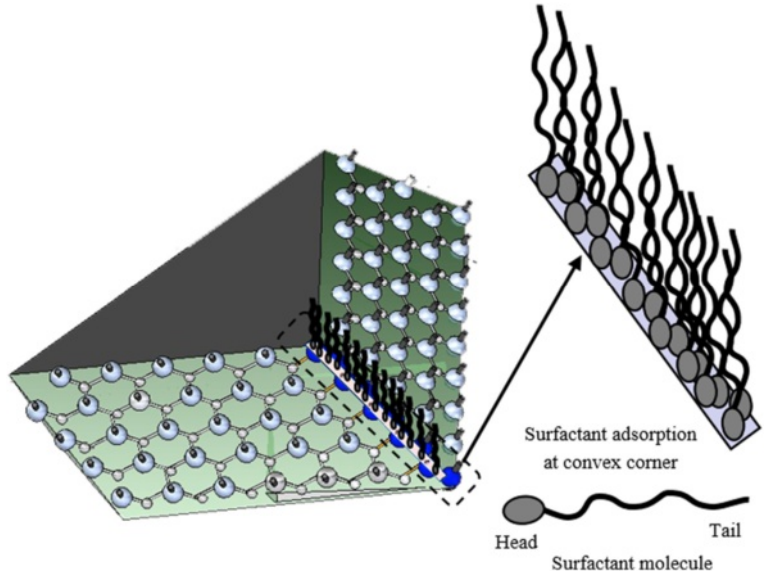

Figure 14 Schematic representation of the surfactant adsorption at the silicon atoms of the convex corners, which belong to {110} planes, in surfactant-added TMAH solution during etching process. The dense layer of surfactant molecules protect the convex corners from etchant that result in the reduction of undercutting.

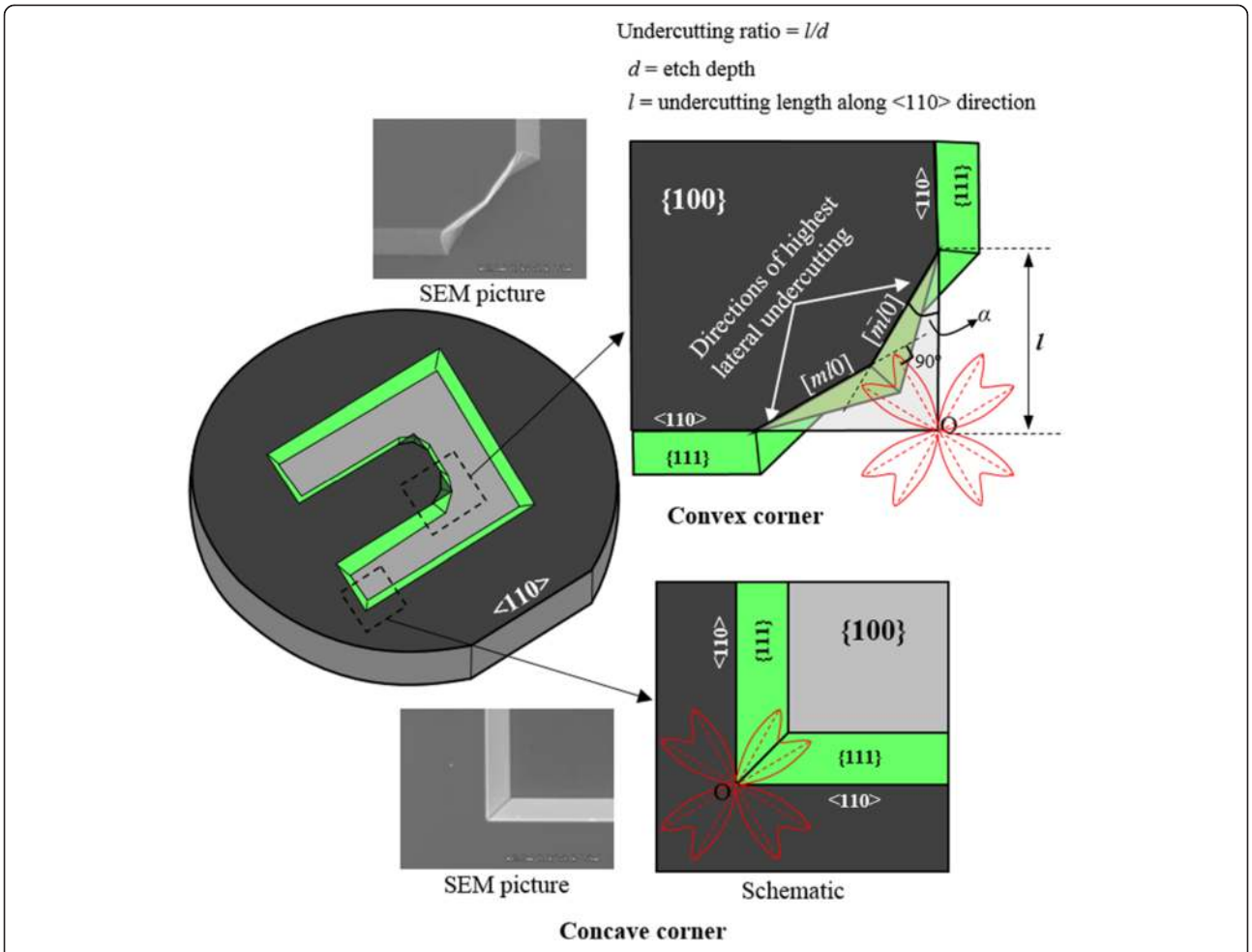

Figure 15 Schematic representation of corner undercutting using lateral underetching diagram.

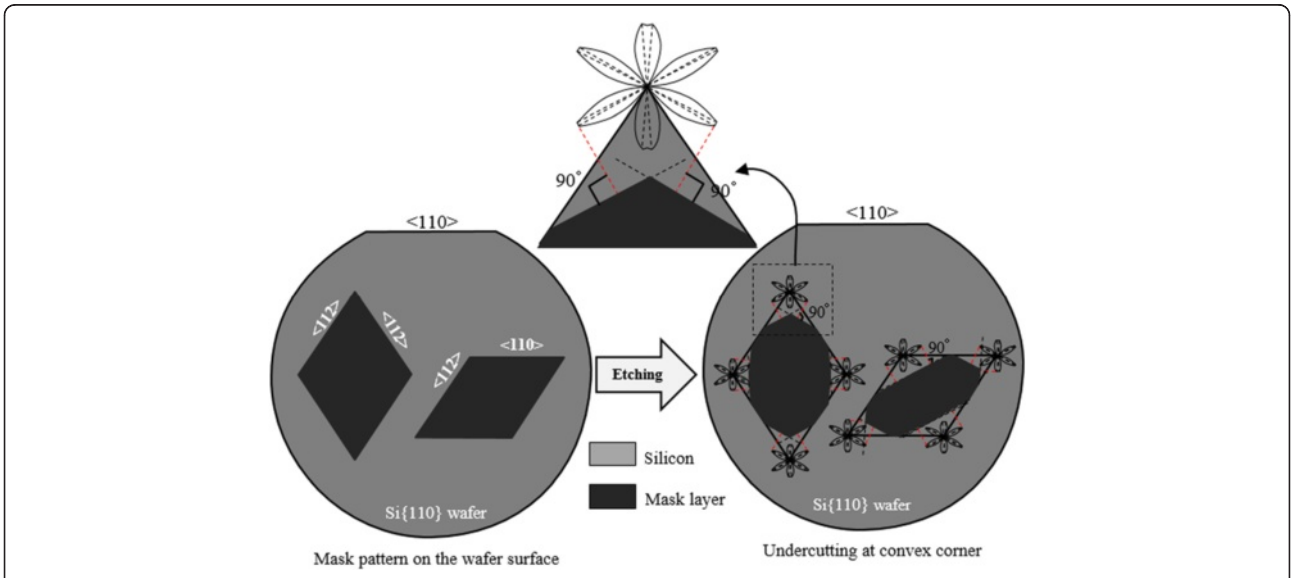

Figure 16 Determination of the etch front of convex corners on Si{110} using lateral undercutting diagram.

types of corners as can be seen in Figures 7, 8, 15 and 16.

The etched profile of the sidewalls appearing at the masked edges can easily be determined using Wulff-Jaccodine method [4,38,165]. In this method, the etched profile is estimated by the distribution of the etch rate vectors existing in the planes belonging to the mask edge from where the etched sidewall profile will appear. The mask edge (or line) is called the zone axis of the planes passing through it. A zone is a set of {hkl} planes that mutually intersect along (or are parallel to) a common direction (or axis) [uvw] with respect to a given crystal as illustrated in Figure 17. The line of intersection [uvw] is called a zone axis. The etch rates of the planes of any zone axis can be determined by the etch rate data of hemisphere [34,38]. The sidewall profile of the etched pattern at the masking edge is the minimal envelop of all intersecting lines which are perpendicular to the etch rate vectors of the different planes belonging to the mask edge (zone axis) as demonstrated in Figures 18 and 19. The planes appearing at the mask edge are the minimum etch rate planes between the horizontal plane and vertical plane at that edge. Similarly the etched profile of undercut structure are estimated. In this case, the sidewalls are the minimum etch rate planes at the maximum lateral underetch rate directions.

The orientation of the facets appearing at the convex corners mainly depend on types of etchant, concentration and additives [79-87]. The etching time and temperature also affect the shape and orientation of

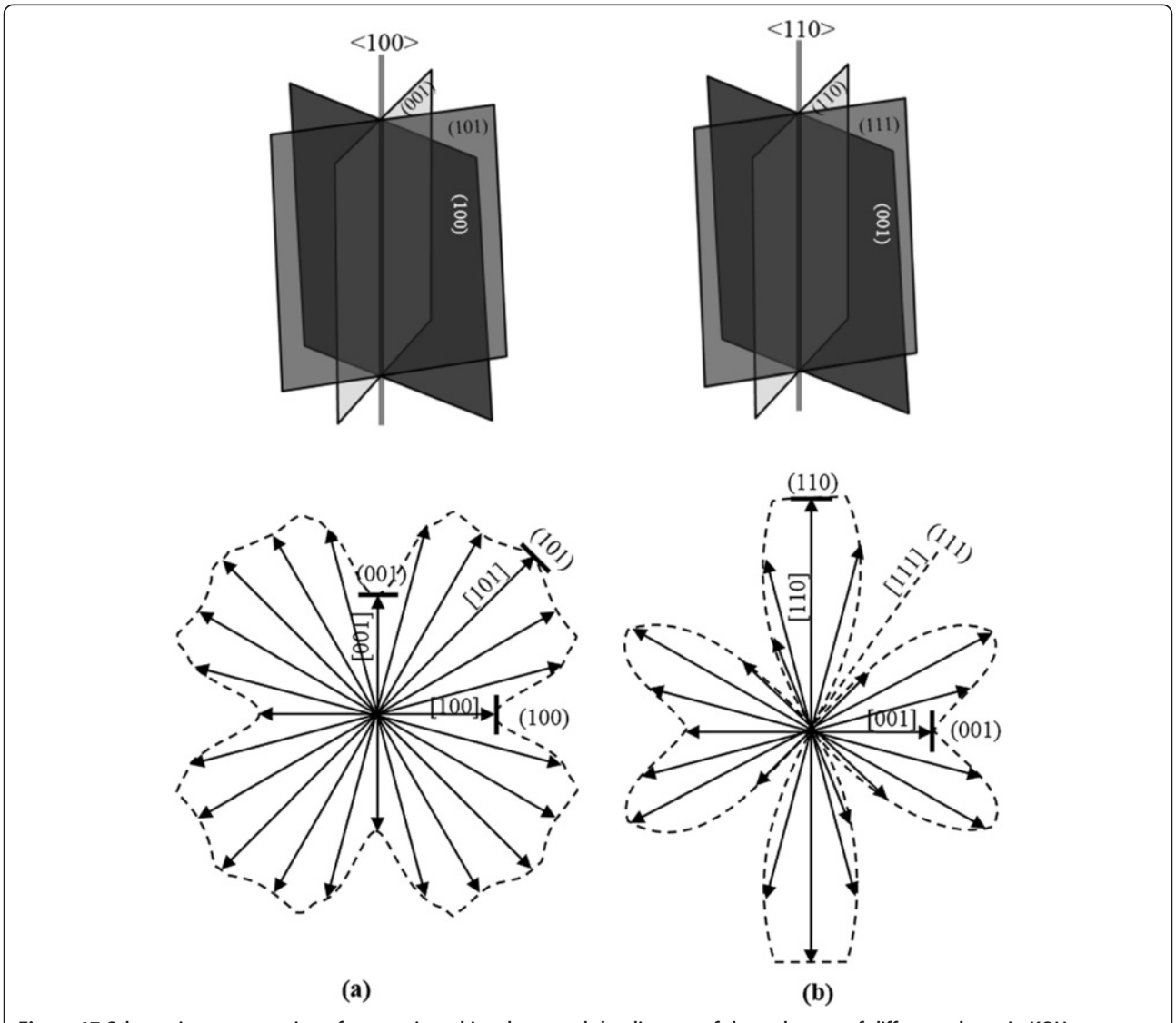

Figure 17 Schematic representation of zone axis and its planes and the diagram of the etch rates of different planes in KOH type etchant for (a) <100> –zone and (b) <110>–zone which are utilized to predict the shape of etched profile using Wulff-Jaccodine method [4].

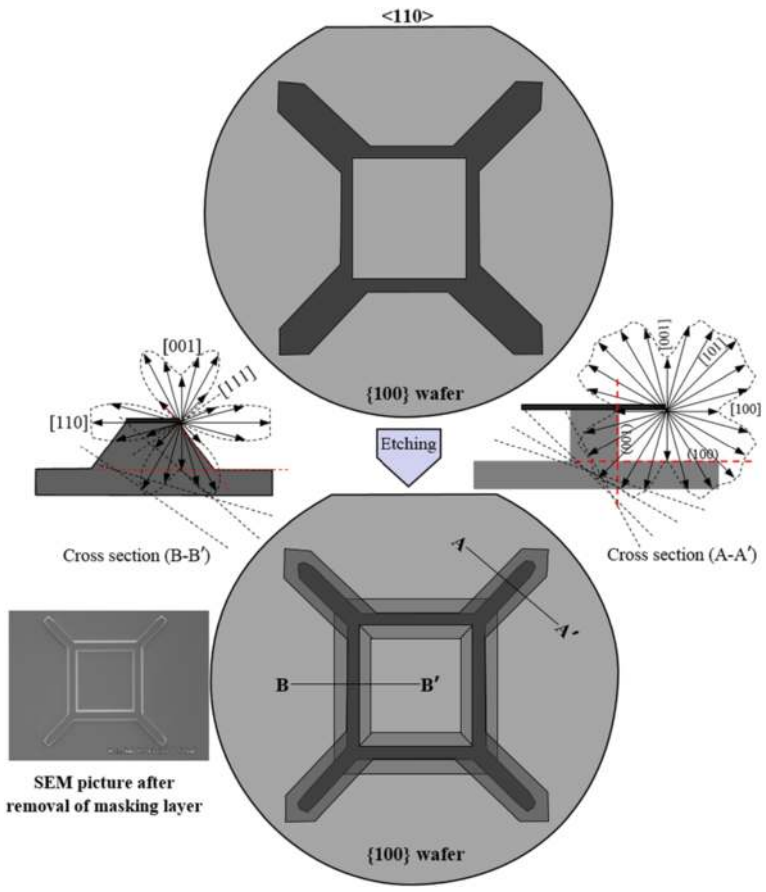

Figure 18 Schematic demonstration of Wulff–Jaccodine method to estimate the etched profiles at the mask edges aligned along <110> and <100> directions on Si{100} surface.

beveled planes. In general, these facets in the case of {100} surface are typically {311}, {211}, {331}, {411}, {212}, {772}, etc. [80-85,90]. The orientation of the undercutting planes significantly affected by the additives in the etchant, for example, IPA in KOH (Figure 11) and the surfactant in TMAH (Figure 12). However the orientation of beveled planes at undercut corners depend on the choice of etchant and its concentration, different research groups have reported different indices for same etchant. For instance in KOH solution, the beveling planes at the convex corners reported by, Shikida *et al.*, Chang Chien *et al.* and Mayer *et al.* are {311}, {772} and {411}, respectively [83,84,92]. Hence, there is some disagreement in the literature about the exact orientation of planes that emerge at the convex corners during etching process. Shikida *et al.* explained that the

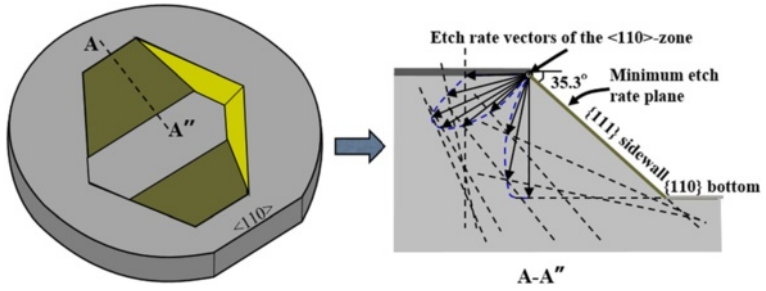

Figure 19 Schematic illustration of the estimation of sidewall profile at <110> mask edge on Si{110} surface using Wulff–Jaccodine method.

fast etching planes emerging at convex corners are located at the saddle point in the etch rate diagram [83]. The location of the saddle point in the etch rate diagram depends on the etching parameters, for instance, it is located around {311} plane for 34 wt% KOH. In the case of {110} wafers, the etch front planes at the undercut convex corner of the mesas structures formed by <112> direction estimated by Kim and Cho for KOH are {311} and {771} planes for acute and obtuse corners, respectively [116]. The beveled angle (α) (Figure 15) vary from structure-to-structure on same sample [80]. Therefore the index of beveled facet will also change. Consequently, the index of the undercut plane for an etchant cannot be defined absolutely. In principle, the undercutting takes place due to the exposure of low coordination atoms with high removal rates, but the facets at the undercut corners are not the highest etch-rate planes. Instead, they are local maximum etch-rate planes, which lie in the vicinity of the saddle point in the etch-rate contour map [166]. In the surfactant-added TMAH and IPA-added KOH, the etch rates of {110} and its vicinal planes are suppressed to considerably low level. Due to this factor, the undercutting at extruded corners, curved and non-<110> edges on {100} surface is significantly reduced [136-146]. It may be emphasized here that the surfactant-added TMAH is not suitable for the fabrication of microstructures on {110} wafer as the etch rate of {110} orientation is very low as presented in Figure 12. As will be discussed in next section, knowledge of the beveled planes is not significantly important to fabricate protected convex corners. The undercutting ratio (l/d) and beveled angle (α), as illustrated in Figure 15, are primarily required to develop a method to realize well-shaped convex corners.

Fabrication methods of convex corners

A significant amount of research has been devoted for the realization of convex corners on Si{100} surface as this orientation is most extensively used in MEMS fabrication [24,88-114,118-126]. However, much less is reported for Si{110} as it is employed only for specific applications [115-117,127,128]. In this article, the fabrication of convex corners are reviewed for both types of orientations (i.e. Si{100} and Si{110}). Several techniques have been developed for the formation of protected convex corners using wet anisotropic etching. Each fabrication technique has its own set of advantages and disadvantages in terms of process flexibility, time, cost and the quality of fabricated corner. These methods are described in following sections.

Corner compensation technique

In order to realize the well-defined convex corners, corner compensation is a most popular method. This method is based on the addition of extra geometry at the convex corner in order to delay the etching so that no undercutting can start at the corner. The corner compensation technique in wet anisotropic etching is covered by a large amount of publications in the past [24,88-126]. Most of the studies are carried out for pure and IPA-added KOH solutions. Some of them are performed for EDP [89,90] and TMAH [108,120,122]. Various types of compensation patterns employed for the realization of convex corners on {100} and {110} silicon wafers are shown in Figures 20 and 21, respectively. The design methodology of these structures are elaborated in the subsequent subsections. The size of the compensating geometries strongly depends on the etch depth and the etching characteristics of the etchant. Various parameters must be known for the analysis and the accurate design of the compensation geometry: etch rate of wafer surface plane (i.e. $R_{\{100\}}$ or $R_{\{110\}}$); etch depth (d); undercutting length (l); beveled angle (α) i.e. an angle between the direction of maximum lateral undercutting and mask edges; undercutting ratio: ($U_r = l/d$).

Corner compensation geometries for Si{100} wafer

The design methodology of corner compensation geometry is same for all types of anisotropic etchants. The dimensions and shapes are analyzed by relative etch rates of crystallographic planes. However different kinds of compensation geometries, as presented in Figure 20, are proposed, four types of designs, namely, triangle, square, <110> band and <100> oriented beam are the basic structures. Other shapes are the derivatives of these structures.

(i) Triangle: The triangular shape geometry, as shown in Figure 22, is a simplest compensating design in terms of determining its shape and dimensions [90,91,120]. In order to calculate the dimensions of the compensating triangle, the undercutting length along the <110> direction (OP, or OC, or l in Figure 22) and the beveled angle $\alpha = \angle OPB = \angle OCB = \angle APO = \angle ACO$ are needed. The lines PB and CB are representing the intersection of the beveling planes with the wafer surface if no compensating pattern is used. The sides of the triangle AP and AC are chosen to coincide with the <lm0> family of lines corresponding to PB and CB. In other words, the sides of the triangle are the highest lateral etch rate directions on {100} surface as illustrated using a red color diagram of lateral etch rates whose center is matched with the convex corner. The length of the sides of the compensating triangle (i.e. AP or AC) can be determined using the law of sines (or sine rule) as follows:

$$\frac{AP}{\sin 135} = \frac{l}{\sin\left(\frac{90-2\alpha}{2}\right)} \quad \Rightarrow AP(or\ \mathrm{AC}) = \frac{l}{\sqrt{2}\sin(45-\alpha)} \qquad (2)$$

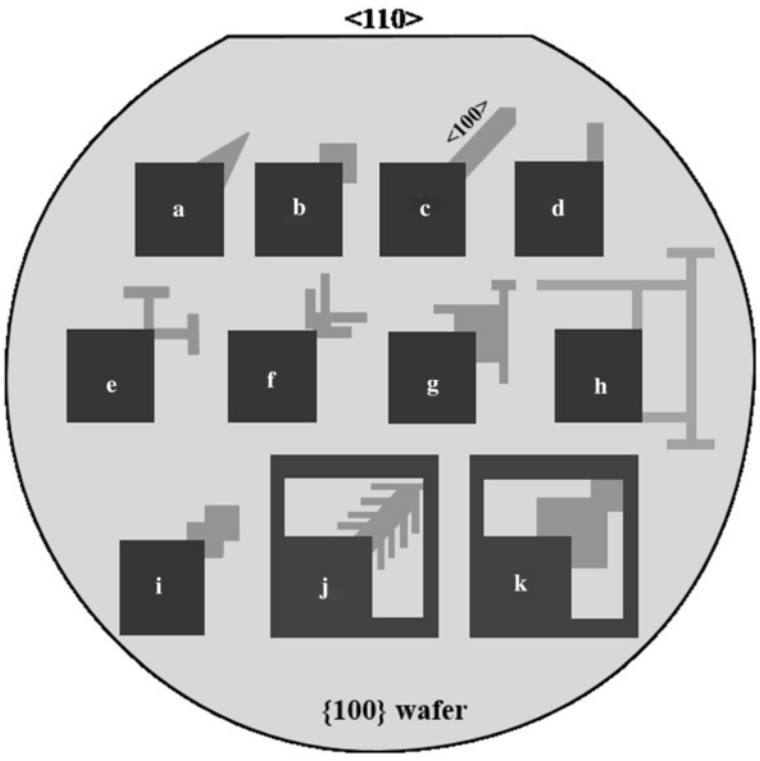

Figure 20 Various types of corner compensation geometries used to realize the convex corners on Si{100} wafer.

It is clear from this formula that the length of the sides of the compensating triangle depends on the undercutting length l and the beveled angle α. The angle α and the undercutting ratio ($U_r = l/d$) depend on the type of etchant. Thus, in order to determine the dimensions of compensating triangle to fabricate a protected convex corner for etch depth d, the length l and an angle α for an etchant must be known. The successive consumption of compensating design during etching is shown by dotted lines.

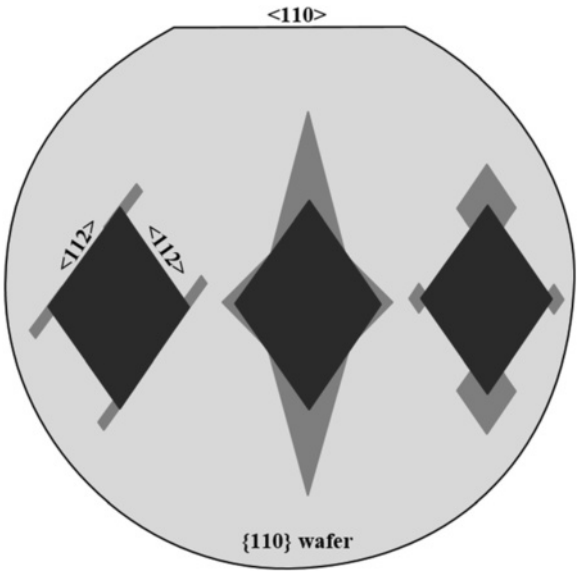

Figure 21 Different kinds of corner compensation designs employed to fabricate the convex corners on Si{110} wafer.

The SEM pictures of mesa structures fabricated in 40 wt% KOH and 25 wt% TMAH using triangular patterns are shown in Figure 23(a) and (b), respectively. In the case of 25 wt% TMAH, the convex corners of the mesa structure are formed with slight beveling at the top side, while in 40 wt% KOH extrusion at the fabricated corner is clearly visible. Hence the triangular compensation geometry does not ensure complete compensation of the convex corners.

In several studies, it is found that the 25% TMAH is the most favorable choice for the minimization of undercutting at sharp convex corners and achieving smooth surface finish with reasonable etch rate of Si{100} by adding a small amount of surfactant [134-137,141,142,146]. Figure 24 shows the SEM image of consecutive etch shapes of mesa structure with triangular compensation structure. It can be noticed in Figure 24(b) that the compensating structures at the top part of the corners have been consumed. However the convex corners have not acquired the desired shape as lot of lump mass is left at the edges of the corners. Although further etching has removed the extruded structure,

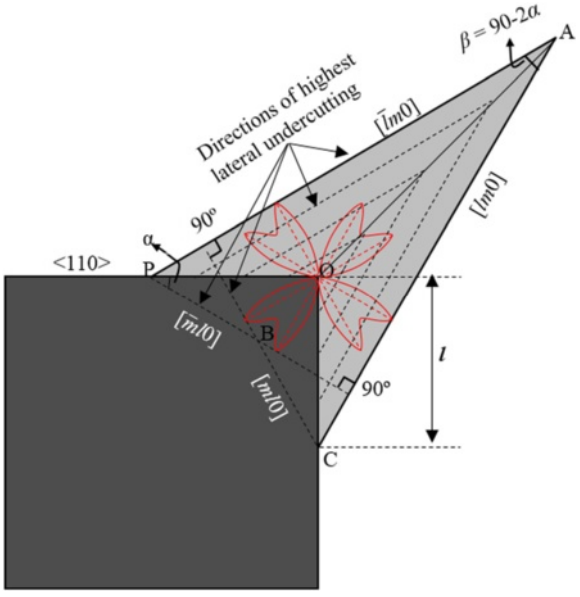

Figure 22 Schematic representation of triangular shape compensation geometry.

the upper side shape of the corner is distorted. From these results, it can be concluded that triangular shape geometry cannot provide a sharp convex corner in surfactant-added TMAH solution.

(ii) Square: The triangular shape geometry require more space to its long sides. In this scheme, square shape design is proposed to reduce the spatial requirement to fit in lesser space at the target corner in comparison to triangular shape as shown in Figure 25. In this case, a square whose center coincides with the apex of the convex corner is used for the time delayed etching to protect the convex corner [24,88,89,91,120,122,125]. It can be noticed from Figure 25 that the square shape compensation design contains three convex corner (m, n and T) and therefore this structure is consumed by the undercutting that starts from these corners. In order to determine the side length of the compensation geometry (a) for etch depth d, a simple formula can be derived using geometrical relations. The calculation is based on the time required for beveled edge $[\bar{l}m0]$ (or <lm0>) to evolve from point m to point O as illustrated in Figure 25.

The perpendicular distance r from a point m($-a/2$, $a/2$) to a line OS which is parallel to $[\bar{l}m0]$ (or <lm0>) and passing through 'O' (*i.e.* $y = \tan\alpha.x$)

$$\mathrm{r} = \frac{\frac{a}{2} - \tan\alpha.\left(-\frac{a}{2}\right)}{\sqrt{1+\tan^2\alpha}} \quad \Rightarrow \mathrm{r} = 0.5a(\cos\alpha + \sin\alpha) \tag{3}$$

The relation between r and l is $l = \frac{r}{\sin\alpha}$

Using these two equations, we can get a relation between a, r and undercutting ratio ($U_r = l/d$)

$$U_r = \frac{l}{d} \qquad \Rightarrow d = \frac{0.5a(\cos\alpha + \sin\alpha)}{U_r \sin\alpha} \tag{4}$$

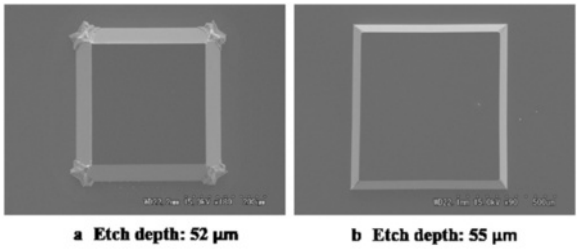

Figure 23 SEM pictures of mesa structures fabricated in (a) 40 wt% KOH and (b) 25 wt% TMAH at 70°C using triangular shape compensating geometry shown in Figure 22.

The mesa structures fabricated in 40 wt% KOH and 25 wt% TMAH using square compensating geometry are presented in Figure 26(a) and (b), respectively. In both cases, the shape of the corners are damaged and significant beveling can be observed. The SEM images of a mesa structure etched in surfactant-added 25 wt% TMAH for different durations are shown in Figure 27. In this case also, the fabricated convex corners are not well-shaped. If the etching is done till the compensating geometry consumed, lot of extruded silicon remains at the corners as can be seen in Figure 27(b). Similar to triangular shape compensation, further etching to remove the extra mass at convex corner alters the desired shape of the corner as shown in Figure 27(c).

(iii) <110> oriented beam: The main objective behind the design of compensation structure is to reduce the spatial requirement and to achieve well-shaped convex corner. In this case, a simple <110> oriented beam (or rectangle) as illustrated in Figures 20(d) and 28 or the combination of <110> oriented beams and squares as shown in Figure 20(e)-(h), is added at the convex corner, [89,94-99,110,120,126]. The progressive etched profiles of simple and asymmetric <110> beams are shown by dotted lines in Figure 28. The consumption of <110> compensation beam takes place by the initiation of undercutting at its convex corners which is illustrated using the lateral etch rates diagrams shown by red color lines. It can be observed from the etched front indicated by dotted lines, <110> beam type compensation design exhibits significant beveling, depending on the beam's

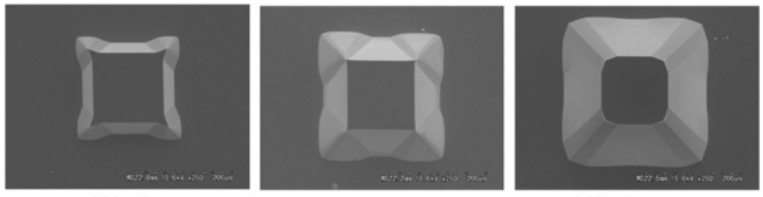

Figure 24 Sequentially etched shape for a mesa structure with triangular shape compensating design in surfactant added 25 wt% TMAH [120]. With permission from Elsevier, Copyright 2009.

width. In order to reduce the beveling, the width of the beam should be as small as possible. The beveling can also be minimized using asymmetric shape beam, as shown in Figure 28(b). Let W and $L_{<110>}$ are the width and length of the compensation beam, respectively. A mathematical relation between these dimensions and the etch depth d can be determined using simple geometrical formulae as employed for the square compensation geometry in previous section. In this case, the perpendicular distance r is calculated from point B to a line OG which passes through 'O' (*i.e.* $y = cota.x$). The following relations are obtained for two differently shaped beams (i.e. symmetric and asymmetric):

(a) Simple beam (Figure 28(a))

$$d = \frac{0.5W\cos\alpha + L_{<110>}\sin\alpha}{U_r} \quad for\ L_{<110>} \geq 0.5W \quad (5)$$

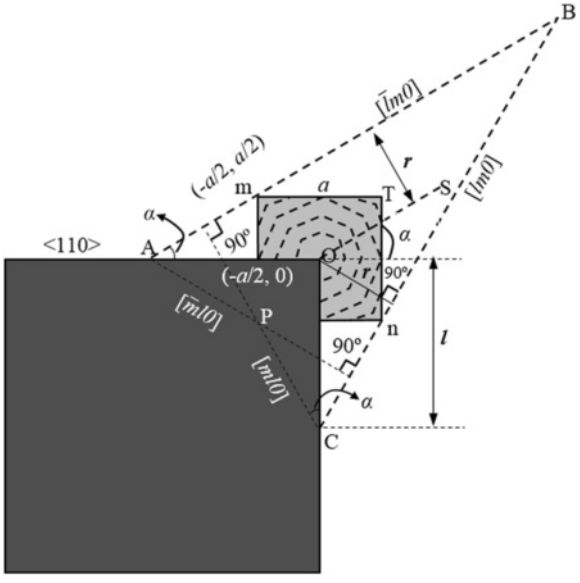

Figure 25 Schematic view of square shape compensation design.

(b) Asymmetric beam (Figure 28(b))

$$d = \frac{W\cos\alpha + L_{<110>}\sin\alpha}{U_r\sin\alpha} \quad (6)$$

The SEM pictures of mesa structures fabricated using asymmetric <110> beam (Figure 28(b)) in 40 wt% KOH and 25% TMAH are presented in Figure 29(a) and (b), respectively. It can be easily noticed from SEM images that the corners are in very bad shape in both etchants. A lump mass extruded along the <110> direction is clearly visible in the case of structure realized in 25 wt% TMAH. Therefore, this compensating design is not suitable for achieving sharp corners in any kind of etchant. As we discussed earlier, the triangular and square shapes compensating geometries are not appropriate for the formation of sharp corner in surfactant-added TMAH. In this case also, it can be easily estimated that the etched shape of the convex corner using <110> beam will also result in extruded mass around the convex corner, but along the <110> directions only.

(iv) Simple <100> oriented beam: None of the compensation structures discussed so far (i.e. triangle, square, <110> –beam) provides sharp edge convex corner. In continuation of the efforts to fabricate sharp convex corner, a simple <100> oriented beam is proposed as presented in Figure 30 [92,100,103,105,108,109,120,122,125]. As shown by dotted lines, the beam is consumed by

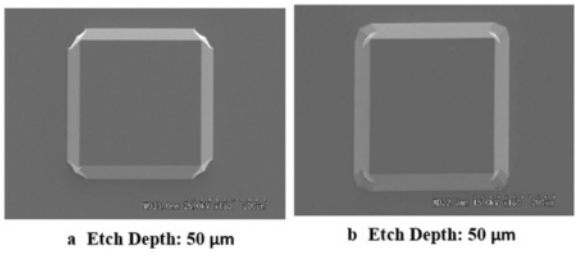

Figure 26 SEM pictures of mesa structures fabricated in (a) 40 wt% KOH and (b) 25 wt% TMAH at 70°C using square shape compensating geometry as shown in Figure 25.

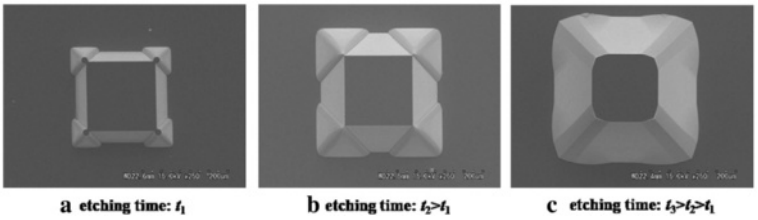

Figure 27 Sequentially etched shape for a mesa structure with square compensating patterns in surfactant added 25 wt% TMAH [120]. With permission from Elsevier, Copyright 2009.

undercutting initiated from the free end and the lateral undercutting that starts at the long edges of the beam.

The etched profile of <100> beam depends on the etching characteristics of different planes appearing at <100> mask edge. These planes are either {100} or {*ij*0} as illustrated in Figures 31 and 32. To predict the etched profile of <100> beam, different conditions based on the etch rate ratio of {*ij*0} and {100} (i.e. $R_{\{ij0\}}/R_{\{100\}}$) can be defined using Figure 31 as follows:

(a) If $\frac{R_{\{ij0\}}}{R_{\{100\}}} \leq sin\theta$, only {*ij*0} planes will be developed at <100> edges
(b) If $sin\theta < \frac{R_{\{ij0\}}}{R_{\{100\}}} < \frac{1}{cos\theta}$, both (100) and {*ij*0} will expose
(c) If $\frac{R_{\{ij0\}}}{R_{\{100\}}} \geq \frac{1}{cos\theta}$, only vertical (100) planes emerge

The etched shapes corresponding to the conditions (a), (b) and (c) are illustrated in Figure 32(a)-(c), respectively. It can be easily observed in Figure 32 that the <100> compensating geometry provides sharp convex corners only if the condition $\frac{R_{\{ij0\}}}{R_{\{100\}}} \geq \frac{1}{cos\theta}$ is satisfied i.e. the sidewalls possess only vertical {100} planes during etching as demonstrated by the SEM picture and the schematic drawing in Figure 32(c).

In order to get a relation to determine the length of <100> beam (i.e. $L_{<100>}$), the successive etched profile, as shown by black color dotted lines in Figure 30, should be analyzed. The lateral etch rate diagram is used to illustrate the directions of undercutting at the free end and the <100> mask edges. The progressive etched profile in Figure 30 is presented for the

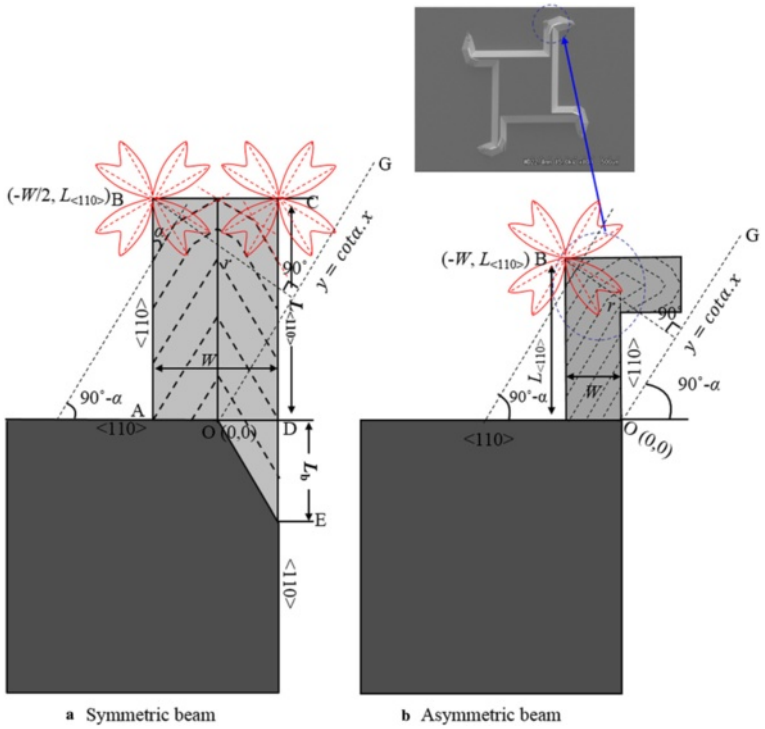

Figure 28 Schematic illustration of <110> oriented compensation geometry.

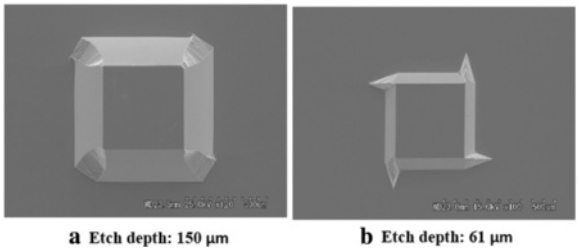

Figure 29 SEM pictures of mesa structures fabricated in (a) 40 wt% KOH and (b) 25 wt% TMAH at 70°C using asymmetric <110> beam compensating geometry shown in Figure 28(b).

condition $\frac{R_{\{ij0\}}}{R_{\{100\}}} \geq \frac{1}{cos\theta}$ as it provides sharp edge convex corner. The undercutting at the free end is caused by fast etching high index planes, while lateral undercutting at <100> edges occurs mainly due to the etching of {100} planes. This design aims to realize the convex corner by the lateral undercutting of {100} planes which appear at <100> edges. For the same reason, the width of the beam should be twice the required etch depth and the beam should be sufficiently long so that the final shape of the convex corner is formed by only the lateral undercutting of {100} planes. In order to determine the beam length (i.e. $L_{<100>}$) to realize a microstructure with well-protected convex corner upto etch depth d (i.e. $\frac{1}{2}W$), a relation between $L_{<110>}$ and d can be developed by formulating the equation of various lines.

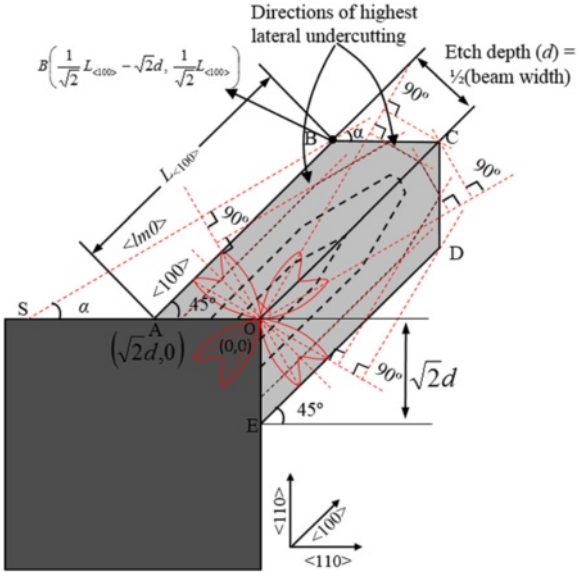

Figure 30 Schematic representation of <100> –oriented compensation pattern.

The equation of a straight line SB (i.e. <*lm*0>, a fast etching front line) passing through the fixed point $B\left(\frac{1}{\sqrt{2}}L_{<100>} - \sqrt{2}d, \frac{1}{\sqrt{2}}L_{<100>}\right)$ and having slope tan α with <110> edge is

$$y - \frac{1}{\sqrt{2}}L_{<100>} = \tan\alpha\left(x - \frac{1}{\sqrt{2}}L_{<100>} + \sqrt{2}d\right)$$
$$\Rightarrow \sin\alpha.x - \cos\alpha.y + \frac{L_{<100>}}{\sqrt{2}}(\cos\alpha - \sin\alpha) + \sqrt{2}d\sin\alpha = 0 \quad (7)$$

The perpendicular distance from a point O (0, 0) to a line SB (i.e. <*lm*0 > direction)

$$d_1 = \frac{L_{<100>}}{\sqrt{2}}(\cos\alpha - \sin\alpha) + \sqrt{2}d\sin\alpha \quad (8)$$

The equation of a straight line AB (i.e. <100> line) passing through a point $A(\sqrt{2}d, 0)$ and making an angle of 45° with <110> edge is

$$x - y - \sqrt{2}d = 0 \quad (9)$$

It can be noticed in Figure 30 that the perpendicular distance from point 'O' to line 'AB' is d (i.e. etch depth). In order to achieve a sharp edge convex corner the beam should be consumed by lateral etching of {100} planes at <100> edges and therefore following condition must be satisfied:

$$d_1 R_{<lm0>} = dR_{<100>} \quad (10)$$

where $R_{<100>}$ and $R_{<lm0>}$ are the etch rates along the directions perpendicular to them.

Substituting the value of d_1 from equation (8) into the equation (10) and re-arranging the terms, we get

$$d = \frac{R_{<lm0>}}{R_{<100>}}\left(\frac{L_{<100>}}{\sqrt{2}}(\cos\alpha - \sin\alpha) + \sqrt{2}d\sin\alpha\right) \quad (11)$$

The microstructures fabricated using <100> beam in 25 wt% TMAH and 40 wt% KOH are shown in Figures 33(a) and (b), respectively. It can be noted from SEM pictures that the microstructures contain well-shaped convex corners. As stated earlier, <100> beam provides sharp convex corner only if the condition $\frac{R_{\{ij0\}}}{R_{\{100\}}} \geq \frac{1}{cos\theta}$ is satisfied. If an etchant (or etching conditions) does not satisfy this relation, triangular (or square) shape can be a better choice. The etching in the surfactant-added TMAH (or IPA-added KOH) exposes {110} planes at <100> edges as shown in Figure 32(a) and therefore this type of etchants are not suitable to fabricate sharp convex corners using <100> beam as compensation geometry [120,133,146].

(v) Superimposed squares: The major part of the research in corner compensation method has been focused

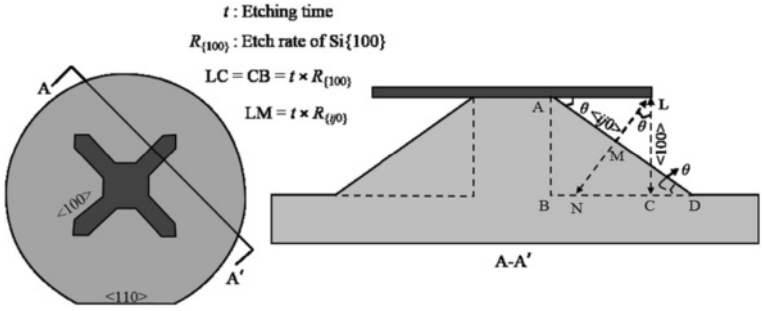

Figure 31 An square shape mask pattern with <100> compensation design. The cross sectional view of the etched profile of the compensating structure is utilized for analyzing the conditions for the exposure of {*ij*0} planes during etching which is presented in next Figure 32.

to reduce the spatial requirement without compromising on the quality of convex corner. The spatial requirement for a particular etchant is primarily determined by two factors: the shape of the compensating pattern and the amount of corner undercutting in that etchant. However, <100> –oriented beam compensation design provides very sharp corner, high spatial requirement along its length is a serious concern. In order to reduce the spatial requirement, superimposed square shape design is proposed [107]. In this geometry, one square of side a and two of side $a/2$ are superimposed at the apex of the convex corner, as illustrated in Figure 34. The shape of compensating structure at different steps during etching is designated by dotted lines. In this case, the structure is first consumed by the fast etching planes appearing at its convex corners (i.e. B, D, E, F and H). After a finite

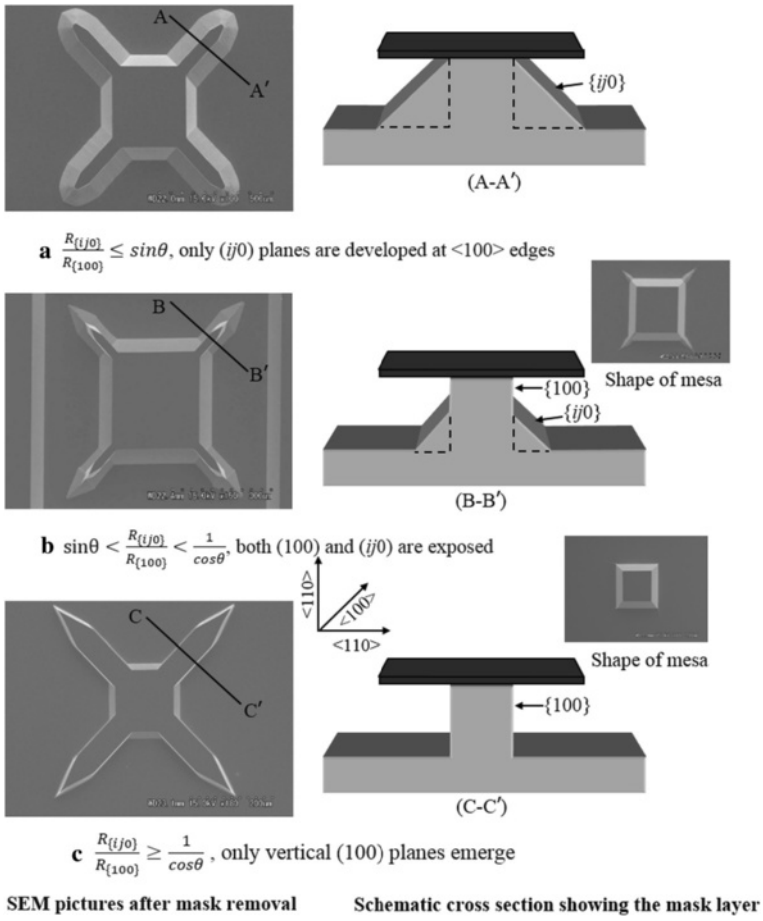

Figure 32 Etched profiles of a <100> oriented beam compensation structure on {100} wafer surface for three different conditions between the angle θ and the etch rates of $R_{\{100\}}$ and $R_{\{ij0\}}$ as illustrated in Figure 31.

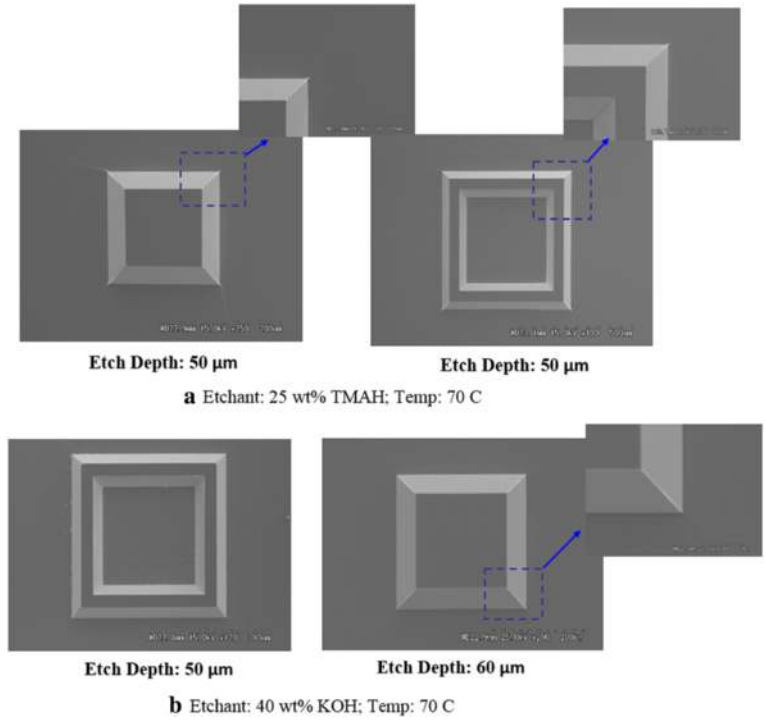

Figure 33 SEM photographs of the microstructures fabricated in TMAH and KOH using <100> oriented compensating beam as shown in Figure 30.

interval of time, depending on the dimensions and etching parameters, the etch front is transformed into a <100> oriented beam whose free end is formed by the <*lm*0> etch front lines as shown in Figure 34(b). After this stage, etching proceeds by both lateral undercutting of the {100} sides and fast propagation of the planes at the free end. Similar to <100> beam, the shape of the convex corner should be taken by the lateral etching of vertical {100} planes as shown in Figure 34(c). In order to get the sharp edge convex corners (i.e. criterion to get the convex corner by lateral etching of vertical {100} planes), the following condition must be satisfied [107]:

$$V\left(=\frac{R_{<lm0>}}{R_{<100>}}\right)<\frac{(3\cos\alpha-2\sin\alpha)(\tan\alpha+1)}{\sqrt{2}} \qquad (12)$$

A detailed derivation of the relation between the square side a and the etch depth d gives [107]:

$$d=\left[\frac{2\sin\alpha+\cos\alpha}{4V}+\frac{\sqrt{2}}{4(\tan\alpha+1)}\right]a \qquad (13)$$

The SEM pictures of mesa structures fabricated in 30 wt% KOH and 25 wt% TMAH are shown in Figure 35(a) and (b), respectively. In both cases, the convex corners of mesa structures are well-defined.

As mentioned, this design relies on the transformation of the etch profile into a <100> beam and the <100> beam is not suitable for the fabrication of convex corners using surfactant-added TMAH. Therefore the compensation geometry formed by superimposed squares is not appropriate to achieve sharp corners in surfactant-added TMAH. Based on the above discussion, it can be stated that none of the compensating designs provides any improvement over the already nearly sharp convex corners obtained in surfactant-added 25% TMAH without compensation as presented in Figure 12(d) [120].

(vi) Corner compensation design for bent V-grooves: The basic problem associated with corner compensation design is the large spatial requirement around the convex corner. In several kinds of microstructures, for instance, the mesa structure surrounded by bent V-grooves and the crossed V-grooves for chip isolation as presented in Figure 36, the space available around the convex corner is less than that is required for the incorporation of compensating structure. In these cases, simple compensation structures (e.g. square, triangle, <100> and <110> beams) cannot be employed as they cannot be fitted in the existing space around the corner. As mentioned earlier, the spatial requirement for a particular etchant is primarily determined by two factors: the shape of the compensating pattern and the amount of corner undercutting in that etchant. Various designs have been reported to fabricate the bent V-grooves.

Mayer *et al.* proposed a design in which <100> oriented beam is fanned out into narrow <110> strips at both sides

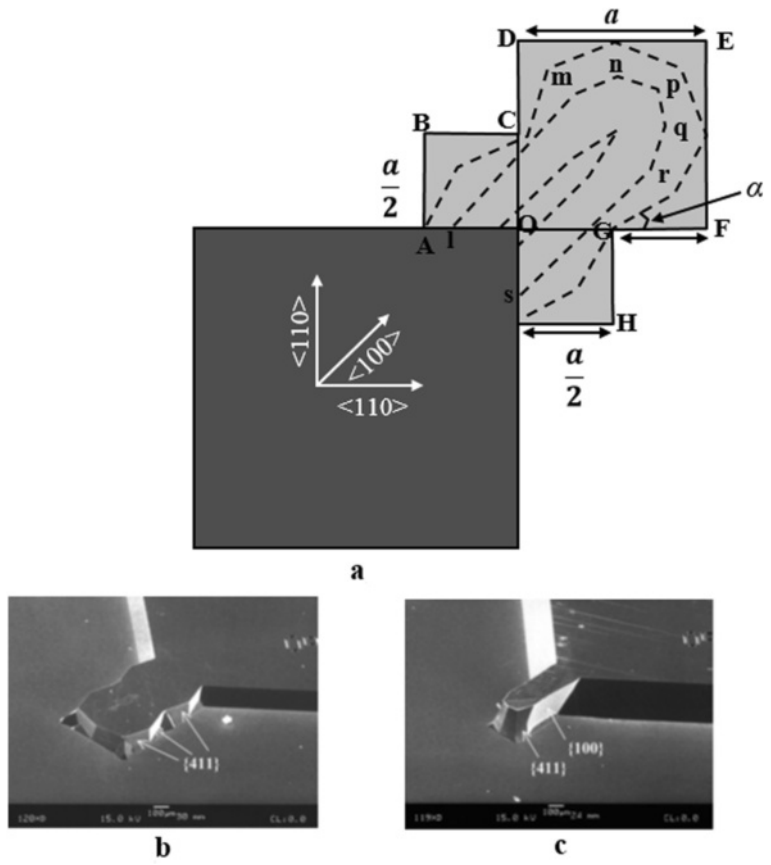

Figure 34 Superimposed squares geometry for corner compensation: (a) schematic; (b) etched profile after time t_1 and (c) etched profile at time t_2 ($>t_1$) when structure transformed to a <100> beam [107]. With permission from IOP, Copyright 2006.

and its free end is connected to the external mask (or frame) by a narrow beam just to eliminate the convex corners as presented in Figure 37 [92]. In this case, the etching of compensation structure starts only from the convex corners at the free end of the <110> narrow beams. As soon as the undercutting from the free end of <110> strips reaches to the main <100> beam, it proceeds by the lateral etching at both sides of the beam. The dimensions of the compensating pattern can easily be calculated using schematic drawing shown in Figure 37(b). The consumption of main <100> beam through lateral undercutting by vertical {100} planes gives $\frac{W_{<100>}}{2}$ etch depth, where $W_{<100>}$ is the width of <100> beam. The length of <110> oriented narrow strips (i.e. $L_{<110>}$) for etch depth d can be calculated as follows:

$$L_{<110>} = \left(\mathrm{d} - \frac{W_{<100>}}{2}\right) \times V \times \frac{1}{\sin\alpha} \tag{14}$$

where $V\left(=\frac{R_{<lm0>}}{R_{<100>}}\right)$ is the etch rate ratio between <lm0> (or the undercut direction at convex corner) and <100> directions.

It is obvious from relation that the length of <110> strips is independent from its width. It depends on the etch depth d, width of the main <100> beam (i.e. $\frac{W_{<100>}}{2}$) and the beveled angle α at convex corner. Hence the width of the <110> strips can be chosen according to convenience. This type of compensating structure can provide the sharp edge convex corner only if the compensation geometry at the end is consumed by only the lateral etching of vertical {100} planes. However, practically the undercut profile of vertical etched profile is distorted by <110> strips that results in the appearance of protruded mass at the bottom of convex corner as can be observed in the SEM images of Figure 37. If the etching is continued to remove this extra mass at the bottom, severe undercutting starts at main convex corners which degrades the shape of the mesa as can be seen in Figure 37(d). Moreover, this method requires more space along the length of the V-grooves and therefore suitable only if the grooves are long enough.

Enoksson made some modifications in the <100> beam as presented in Figure 38 to minimize the problem of high spatial requirement [101]. In this design a

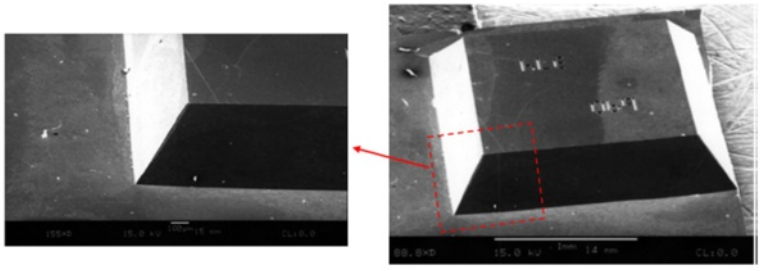

a Etch depth : 379 μm [107]

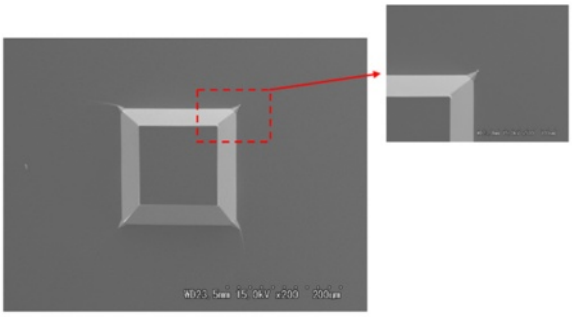

b Etch depth : 50 μm

Figure 35 SEM pictures of mesa structures fabricated in (a) 30 wt% KOH at 80°C (Courtesy of Dr. W. Fan, work done at Peking University) and (b) 25 wt% TMAH at 70°C using superimposed squares as compensating pattern.

narrow slit is incorporated in the middle from the concave corner. The length of the slit must be slightly longer than twice the required etch depth to ensure that the compensating structure is completely underetched. The progressive change in the shape of the compensating structure during the etching process is illustrated by dotted lines. The first half of the beam (i.e. upto point C) is consumed by the undercutting of {100} vertical planes. The undercutting at A-A' and B-B' crosses each other at point 'C' and subsequently the undercutting also start from point 'C'. Similar to simple <100> beam (Figure 30), the width of the beam is chosen twice of the etching depth. Figure 38(b) presents the SEM picture of convex corner fabricated using modified <100> beam shown in Figure 38(a). Though the compensation geometry presented in Figure 38 requires less space in comparison to simple <100> beam (Figure 30), it is not suitable for the fabrication of bent V-grooves. Additionally, it does not provide sharp edge corner as some residue left at the lower part is clearly visible in Figure 38(b).

In order to realize the bent V-grooves, Wacogne *et al.* proposed a design composed of superimposed rectangle and square patterns as shown in Figure 39 [118]. The evolution of the etched profile, initiating from corners B and H, is shown by dotted lines. In this design, the protection time mainly depends on the distance of beveled direction <*lm*0> at point B (or H) from point O as indicated by *r* in Figure 39(b). This can be formulated in terms of beveled angle (α) and the dimensions of the rectangular strip (i.e. length l_1 and width (g_1-g_2)) as done for square and <110> compensation geometries. Furthermore, the distance *r* can be correlated with etch depth *d* and the etch rates of <*lm*0> and <100> (i.e. $R_{<lm0>}$ and $R_{<100>}$) as follows:

$$rR_{<100>} = dR_{<lm0>} \Rightarrow r = d\frac{R_{<lm0>}}{R_{<100>}} \Rightarrow r = dV \qquad (15)$$

The etch rate of a direction means the velocity of the edge during etching along a direction perpendicular to it. Length of the compensation strip can be defined as follows:

$$l_1 = \frac{R_{<lm0>}}{R_{<100>}}\frac{d}{\sin\alpha} - \frac{g_1 - g_2}{\tan\alpha} \qquad (16)$$

This equation is valid only if the length l_1 is greater than the width (g_1-g_2). This is the same case as considered for <110> compensation geometry. Furthermore, the size of square DEFX (or width g_2) should be as small as possible to ensure that it is consumed before the beveling directions <*lm*0> from point B and H reach the main convex corner O. Figure 39(c) and (d) present the shape of bent V-grooves fabricated in 40 wt% KOH at 55°C using the compensation design shown in Figure 39(b). It can be noticed that the perfect compensation is not possible using this design as the deformation

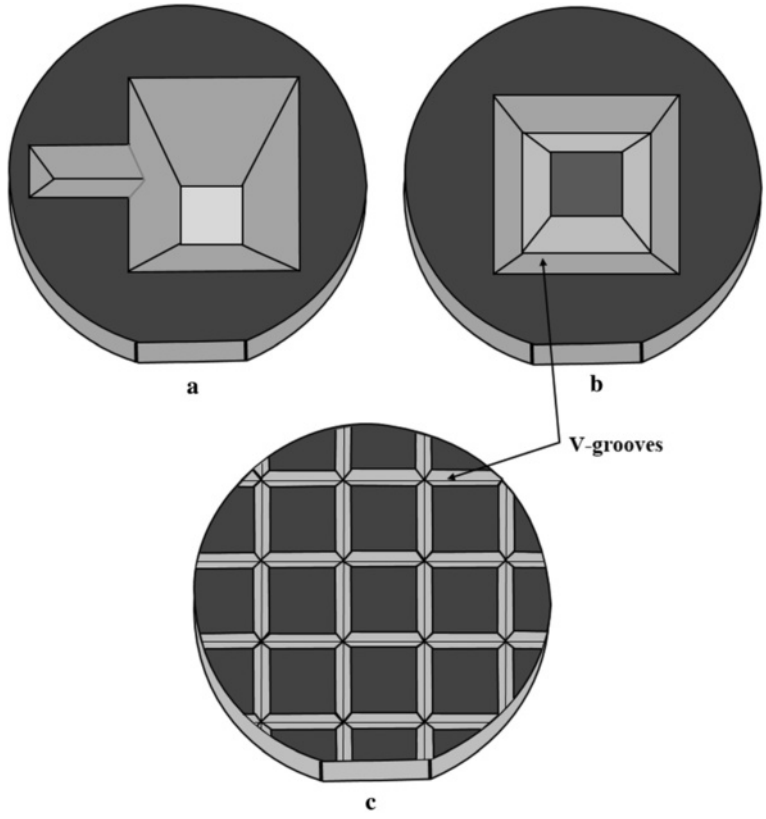

Figure 36 Schematic representation of the wet bulk micromachined structures which have limited space around the convex corners: (a) V-groove connected to square aperture; (b) mesa structure surrounded by bent V-grooves; (c) V-grooves for chip isolation.

of convex corner and some residues of the compensation structure at the bottom of the corner is clearly visible. Moreover this design can be used only if the length of the groove is sufficient for compensation design to fit in the pattern.

The design of a compensation pattern has been a major concern when the space is limited around the corner. In continuation of the efforts to overcome the problem of high spatial requirement and to fabricate well-shaped corners, Scheibe *et al.* proposed superimposed <110> oriented beams, as shown in Figure 40, for the formation of crossed V-grooves for chip isolation [98]. As can be noted from the SEM picture of crossed V-grooves in Figure 40(b), the corners are damaged and some residual mass remains at the bottom surface.

Figure 41(a) shows a compensation scheme for the fabrication of pyramidal aperture connected to V-groove as presented in Figure 36(a). The dotted lines designate the shape of the structure as etching proceeds. The evolving etched profile of compensation pattern clearly indicates that the significant beveling will take place at the convex corners A and B. This beveling can be reduced if the square shape compensation geometry (Figure 41(a)) is replaced by asymmetric <110> beams as illustrated in Figure 41(b). However this design will also not be able to provide the well-defined corners as discussed in section Corner compensation geometries for Si{100} wafer (<110> oriented beam).

In the case of convex corner surrounded by bent V-grooves, it can be concluded that no compensating geometry provides well-protected convex corner if etching is done in pure KOH and TMAH solution. Nevertheless, the investigation of new etchants has improved the situation [120,134-146]. Surfactant-added TMAH is known to provide minimum undercutting at all kinds of corners and edges as can be seen in Figure 12. In different concentration of TMAH, 25% TMAH is the most favorable choice for minimizing the undercutting while achieving smooth surface finish with reasonable etch rate of {100} planes [134-136,140-142,145,146]. In this etchant, any shape of the compensating design can conveniently be fitted in the accessible space for the formation of grooves for chip isolation and bent V-grooves. It means that surfactant-added TMAH eliminates the problem of large spatial requirement. As discussed earlier, surfactant-added THAH is not feasible for the fabrication of convex corners because the planes appearing at the edges of the compensating design have lower etch rates than {100}. If triangular (or square) compensating geometry is employed, the extruded corners towards the

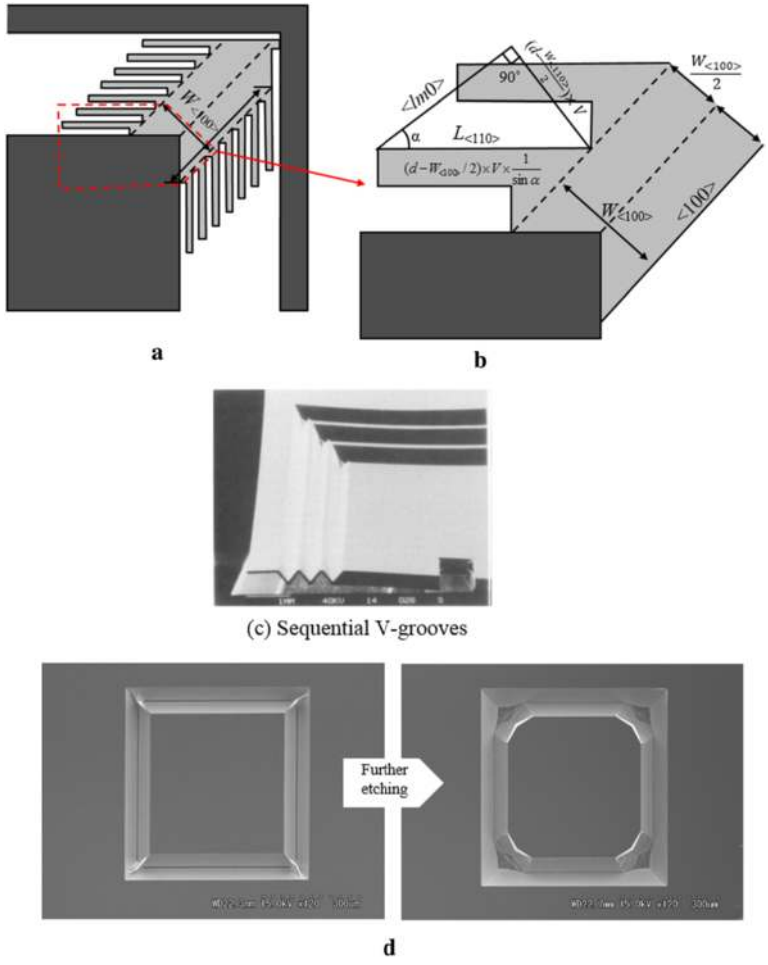

Figure 37 Corner compensation design for the realization of bent V-groove using (a) <100> oriented beam where several <110> oriented narrow strips are added on both sides; (b) Dimensioning of the narrow strips; (c) Sequential V-grooves [92] (with permission from The Electrochemical Society, Copyright 1990); (d) Mesa structures surrounded by bent V-grooves fabricated in 40 wt% KOH.

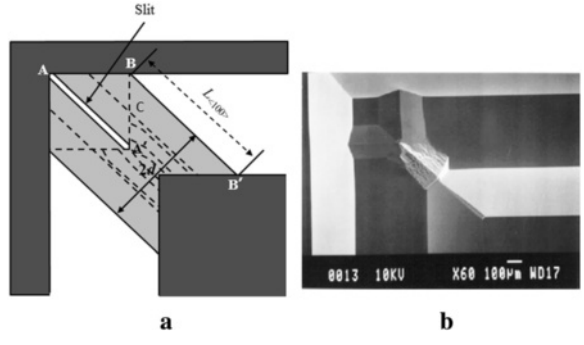

Figure 38 Modified <100> beam: (a) Schematic view and (b) SEM picture of fabricates convex corner using this design [101]. With permission from IOP, Copyright 1997.

bottom side will encounter the opposite {111} planes as a barrier, as shown in Figure 42(a). Therefore, extrusion due to extra silicon at convex corners can be reduced in such structures.

In square and triangular compensating structures, the triangular shape is more convenient due to its simple design. During the etching process, it is consumed while maintaining its original shape. The mesa structure surrounded by bent V-grooves and the grooves for chip isolation fabricated using the triangular shape are shown in Figure 42(a) and (b), respectively. It can be observed in SEM photographs that the convex corners are well-protected. It can be emphasized here that the surfactant-added TMAH is a best choice for the realization of convex corner surrounded with bent V-grooves. As discussed previously, the pure KOH and TMAH are not suitable to fabricate a pyramidal aperture connected to V-groove with well-defined convex corners. The surfactant-added solution is an appropriate choice to fabricate such kind of pyramidal aperture as

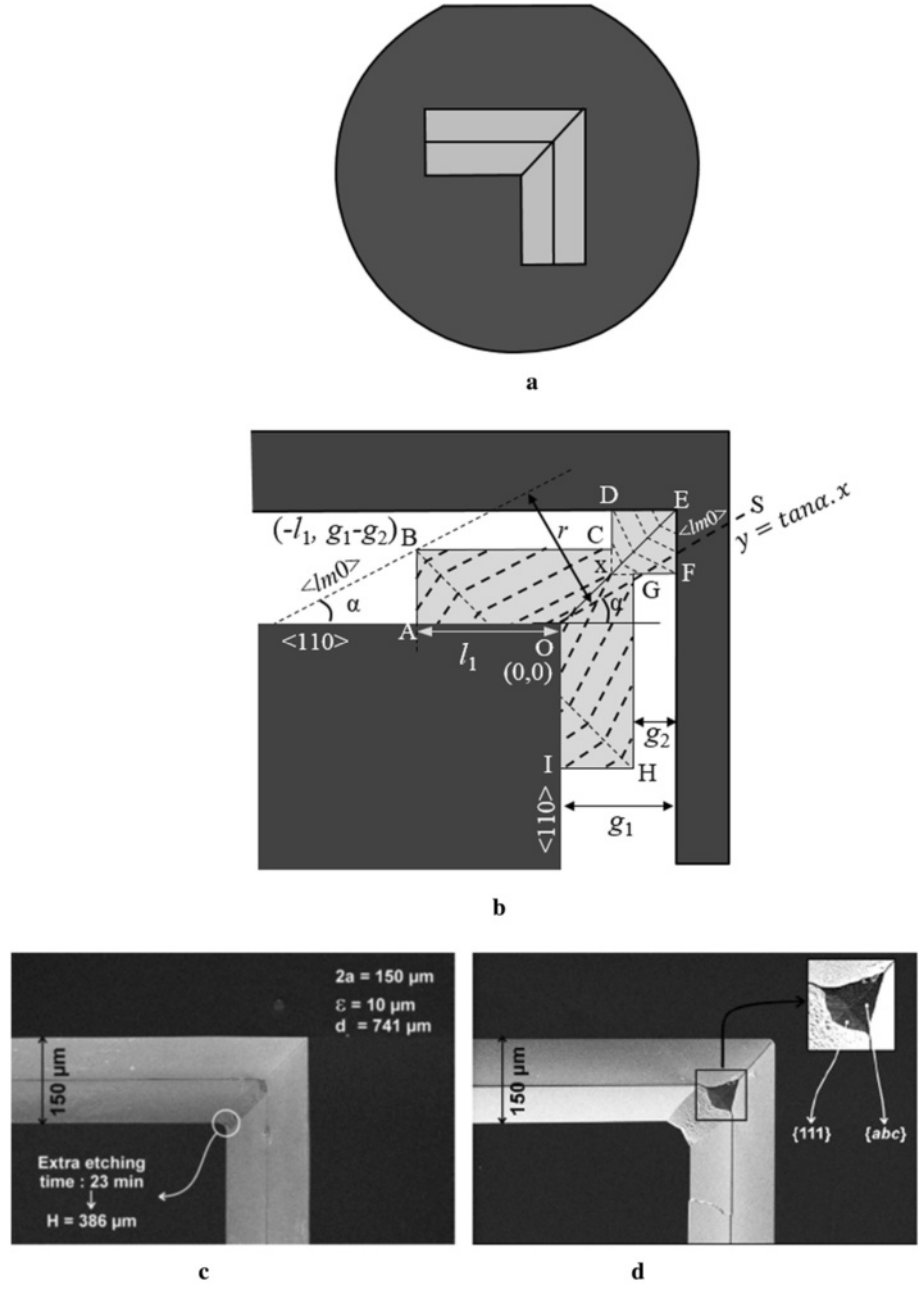

Figure 39 Fabrication of microstructures with bent V-grooves: (a) schematic view of bent V-groove in {100} wafer; (b) mask pattern with corner compensation structure; (c)-(d) fabricated structures [118] (with permission from Elsevier, Copyright 2006).

presented in Figure 43. This kind of structure is frequently required for a wide range of applications, especially in the field of microfluidics and microbiology.

Corner compensation geometries for Si{110} wafer

{110} silicon surface has two fold symmetry and therefore the angle at the sharp corners depends upon the direction at which {111} planes appear as presented in Figures 2(b) and 3(b). Analogous to {100} surface, the undercutting takes place at the convex corner on {110} surface. Therefore, in order to fabricate a microstructure with convex corner on Si{110} wafer, extra structure must be added at the corner for its protection during etching step. In the case of {100} wafers, the compensation structure provides well-defined corner if it is consumed by the lateral etching of vertical {100} planes. However, such kind of etching characteristics is not possible on {110} wafers. Furthermore, {110} wafer is not suitable for the fabrication of MEMS structure using surfactant-added TMAH as it has very low etch rate in

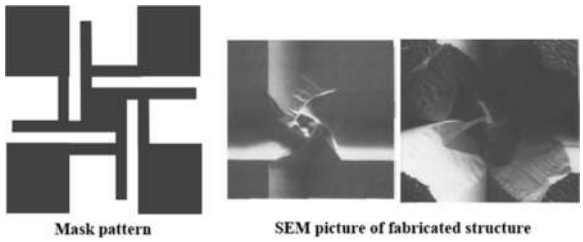

Figure 40 Corner compensation structure for the fabrication of grooves for chip isolation [98]. With permission from IOP, Copyright 1995.

this etchant as presented in Figure 12 [37-40]. In order to protect the corner on {110} wafer, mainly three kinds of compensation geometry, namely, triangular, rhombus, and parallelogramic beam are reported, as illustrated in Figures 21 and 44 [115-117,128]. These designs are studied for the convex corners formed by the intersection of vertical {111} planes (or <112> directions). The design methodology of these geometries are briefly described in following subsections.

(i) **Triangular**: As discussed in the case of {100} wafer, undercut shape of the corner (i.e. beveled angles)

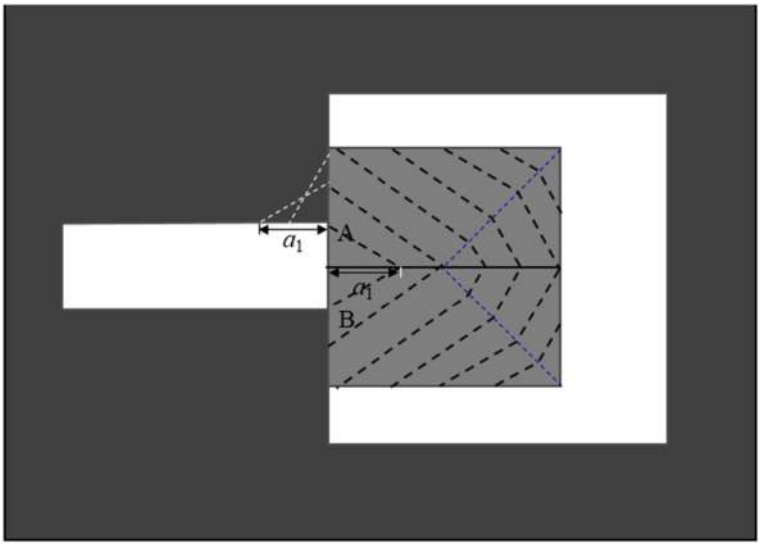

a

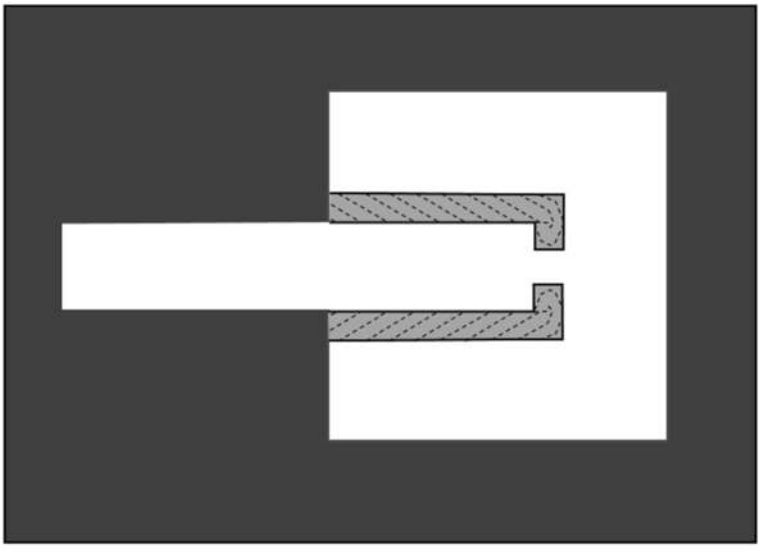

b

Figure 41 Schematic view of mask pattern with compensation geometry to fabricate a microstructure with V-groove connected to a square aperture as shown in Figure 36(a) using different shapes compensation geometries: (a) square shape and (b) asymmetric <110> beams.

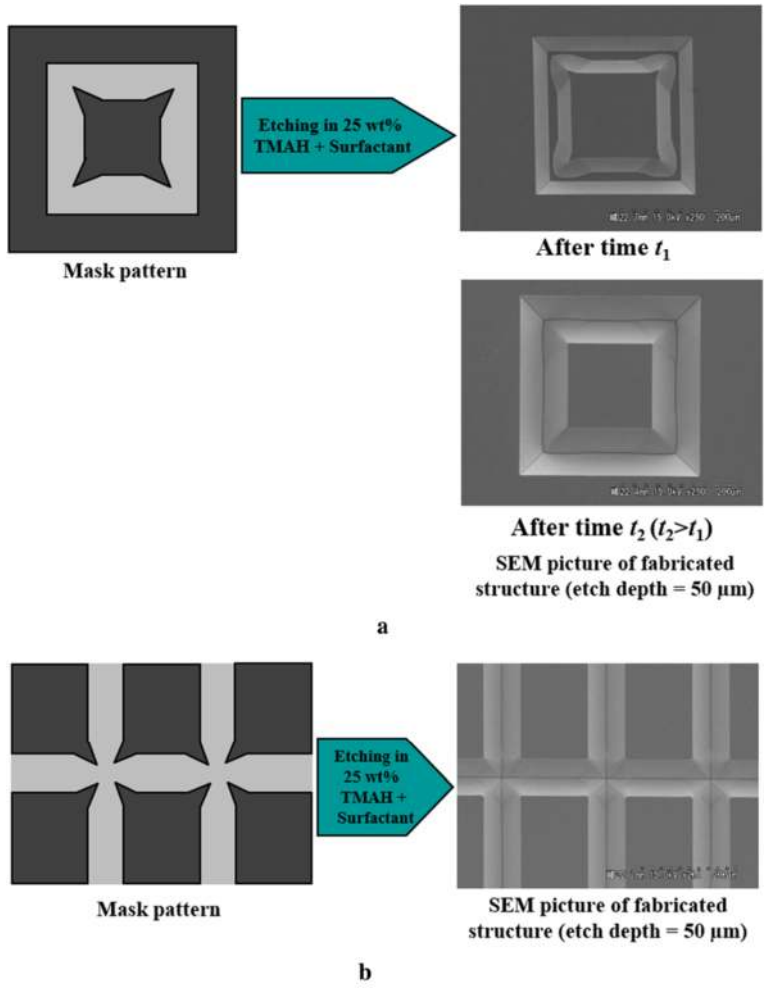

Figure 42 Fabrication of the (a) microstructure with bent V-grooves and (b) grooves for chip isolation in surfactant added 25 wt% TMAH using triangular shape compensation structure [120]. With permission from Elsevier, Copyright 2009.

and the amount of undercutting (i.e. undercutting length l) versus etch depth (d) depend on the etching conditions and vary from etchant-to-etchant. Therefore these parameters must be known to investigate the design of compensating geometry. The concept behind the design of this structure is the same as used for {100} wafer. However the compensation structure cannot be identical for all corners as the included angles at convex corners are not same as can be seen in Figure 44. In this design, the directions of the sides of the triangle at obtuse corners are the same as the directions of undercutting lines at acute corners and vice versa, as shown in Figure 44(a). In the absence of compensation pattern, the beveled shape (or undercut shape) at obtuse and acute angles are shown by red and yellow color lines, respectively. The successive etched profile of compensating pattern during etching is represented by dotted lines. The sides JP' and KP' of the compensating triangle at acute corners are chosen to coincide with <*uuv*> family of lines corresponding to the directions of the undercutting at obtuse corners as indicated by red color lines. Similarly at obtuse corners the sides of the triangle MO' and LO' should coincide with <*llm*> directions which are the directions of undercutting at acute corners as shown by yellow color. In order to calculate the dimensions of the triangle using the sine rule, the beveled angles and the lengths of undercutting along <112> directions at obtuse (i.e. α_o and l_o) and acute (i.e. α_a and l_a) angles must be known. The SEM photographs of acute and obtuse convex corners fabricated using triangular compensation patterns in 42.5 wt% KOH at 80°C are shown in Figure 45(a) and (b), respectively [116]. It can be easily noticed that none of the corners is well-shaped, elongated residues of different lengths are left at both types of corners.

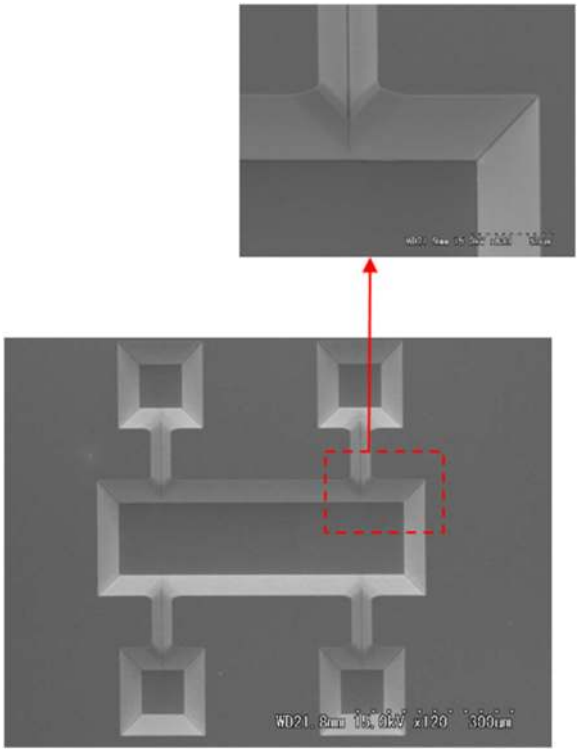

Figure 43 SEM picture of the pyramidal apertures connected to V-grooves.

(ii) **Rhombus (or Square):** This design is a shortened version of triangular shape pattern discussed in previous section. The original idea of this kind of shape is the same as the one reported by Puers *et al*. for the design of square shape compensation pattern for the formation of convex corners on Si{100} [91]. The sides of compensating rhombus aligned along <112> direction. The center of the rhombus coincides with the apex of the convex corners and it is of maximum size which can be inscribed in the triangle as illustrated in Figure 44(b). In the etching process, the compensating rhombus is totally consumed by the undercutting that starts from the three convex corners (A, B and C at acute corners, E, F and G at obtuse corners) as illustrated by the dotted lines in Figure 44(b). The dimensions of the rhombic pattern can simply be calculated using the sine rule as done earlier for other structures. The SEM images of the convex corners fabricated in pure and IPA-added 40 wt% KOH are shown in Figures 46(i) and (ii), respectively [115]. In all cases except acute corner in IPA-added KOH (Figure 46(c)-ii), irregular shape residue can easily be observed.

(iii) **Parallelogramic beam (or Beam):** In this method, a <112> oriented beam (or parallelogramic beam) is fitted at the convex corner. In order to calculate the length of the beam to protect the corner for etch depth d, the undercutting versus etch depth data should be available. As illustrated in Figure 44(c), the length of the compensating beam corresponding to undercutting length l_o (i.e. QX) for etch depth d should be QY. In this design, the beam width does not play any role and it should be as small as possible, but it should not be consumed by the lateral undercutting of {111} planes which appear at its edges. The great feature of this structure is that the same size beams are added at the acute and obtuse corners. The SEM pictures of convex corners fabricated in 42.5 wt% KOH using beam shape compensating geometry are presented in Figure 47(a) and (b), respectively. An SEM image of a cantilever beam with vertical sidewalls in {110} wafer realized in 25 wt% TMAH using this design is shown in Figure 48.

Perfect convex corners using two-step etching techniques

The compensation technique relies on time-delayed etching of convex corners through some added extra geometry. The dimensions of the compensating structures depend on the etch depth up to which the convex corners have to be created. This technique, therefore, requires (a) precise control of etch rate and (b) highly uniform wafer thickness. The convex corner results in damaged corner if the etching is performed more than the prescribed etching time. Moreover, in the corner compensation method, high spatial requirement is a big concern, especially when the spacing between adjacent structures is limited. Hence, achieving very sharp corner without any damage at the convex edge (or any residual at the bottom surface) is a tedious task. In order to avoid these issues and to fabricate microstructures with ideally sharp corners, two techniques have been developed [69,111-113]. The convex corner is formed by the intersection of two {111} planes and, in these techniques, {111} planes are fabricated in two steps. After fabricating one of the two {111} planes of the convex corner, it is protected by masking layer. Thereafter, in the next step of etching, second plane is realized. Hence both methods provide very clean and sharp convex corners, but lithography requires two masks and the wet etching is performed in two steps. The fabrication steps of these techniques are discussed in following subsections:

(i) The process steps of the first technique, which is proposed by Kwon *et al.*, are described in Figure 49 [69]. The fabrication of convex corner is done using two masks. After defining a pattern using mask # 1, anisotropic etching is employed to form a cavity of desired depth (Figure 49(b)). Thereafter masking

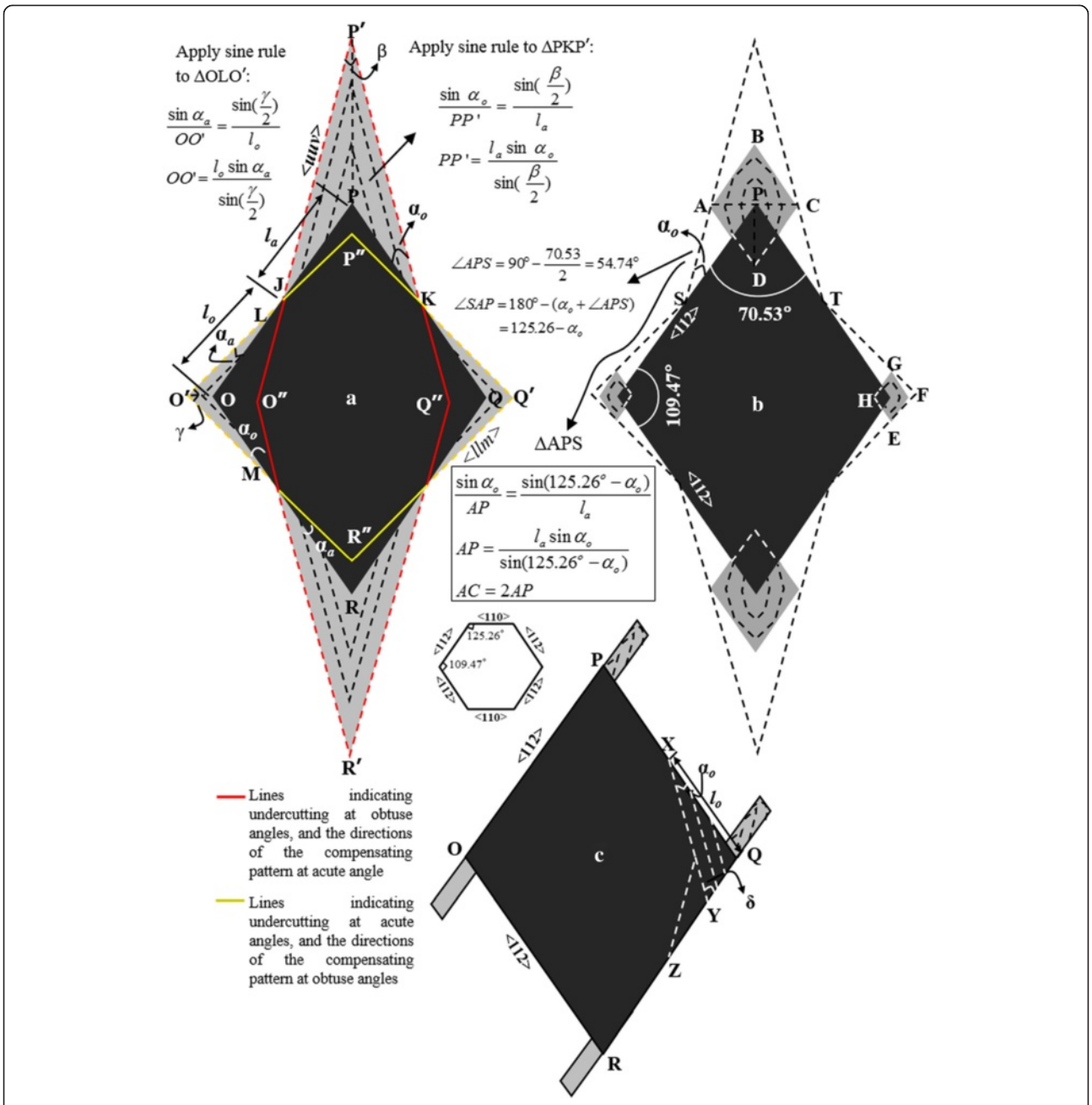

Figure 44 Schematic representation of different shapes corner compensation geometries namely (a) triangular, (b) rhombus or square, and (c) parallelogramic beam for the protection of convex corner during fabrication in {110} silicon wafers [128].

layer is deposited on exposed silicon. The masking layer can be thermal oxide or CVD nitride. If the oxide is used as mask, KOH is not a suitable etchant as it exhibits finite oxide etch rate. In that case, TMAH should be used as an etchant. Subsequent to the deposition of masking layer, second step of lithography is performed using mask # 2 to pattern the masking layer on the sidewalls as well as top surface. Due to uneven surface topography, it is very hard to coat the photoresist of a uniform thickness using spin coating technique [167-169]. The use of standard liquid photoresist deposited by a spin-coating process results in non-uniform thickness, especially on sloping sidewalls and convex edges/corners. At the convex edges, the film may be even discontinuous, as the photoresist reflows from these edges due to surface tension. Very thin or discontinuous photoresist coating at the convex

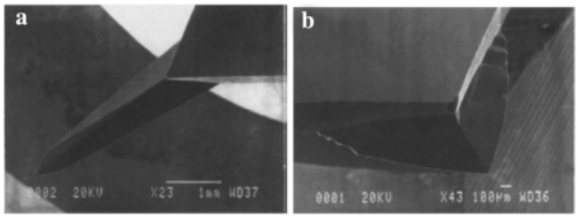

Figure 45 SEM photographs of (a) acute and (b) obtuse convex corners fabricated using triangular compensation patterns in 42.5 wt% KOH at 80°C [116]. With permission from The Electrochemical Society, Copyright 1998.

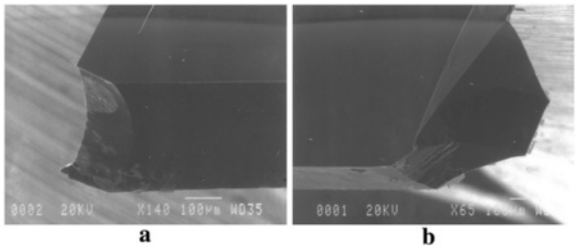

Figure 47 SEM photographs of (a) acute and (b) obtuse convex corners fabricated using parallelogramic beam compensation design in 42.5 wt% KOH at 80°C [116]. With permission from The Electrochemical Society, Copyright 1998.

edges fails to protect the masking layer at the sharp edges during the etching process. This, in turn, leads to etching of silicon during anisotropic etching. Moreover, due to reflow of spin coated photoresist, excessive amount of photoresist is accumulated on the bottom of the cavities/trenches. In order to coat the constant thickness photoresist, spray coating method is employed. The thickness, uniformity and surface roughness of spray-coated photoresist depend on several parameters such as viscosity of the photoresist, orifice of the spray nozzle and the air pressure applied to the nozzle [169-171]. After the patterning of masking layer using second step of lithography (Figure 49(c)), the next step of anisotropic etching is carried out (Figure 49(d)). At last, mask layer can be removed globally if required. An SEM picture of a microstructure fabricated using this method is shown in Figure 49(f) [69]. It can be noticed that the convex corners are well-protected.

However this technique provides protected convex corners, the second step of lithography is onerous as it is performed on 3D surface topography. 3D nature of the microstructure makes it very difficult to transfer the pattern [168,169,171-174]. There are three major issues in lithography process on 3D topography:

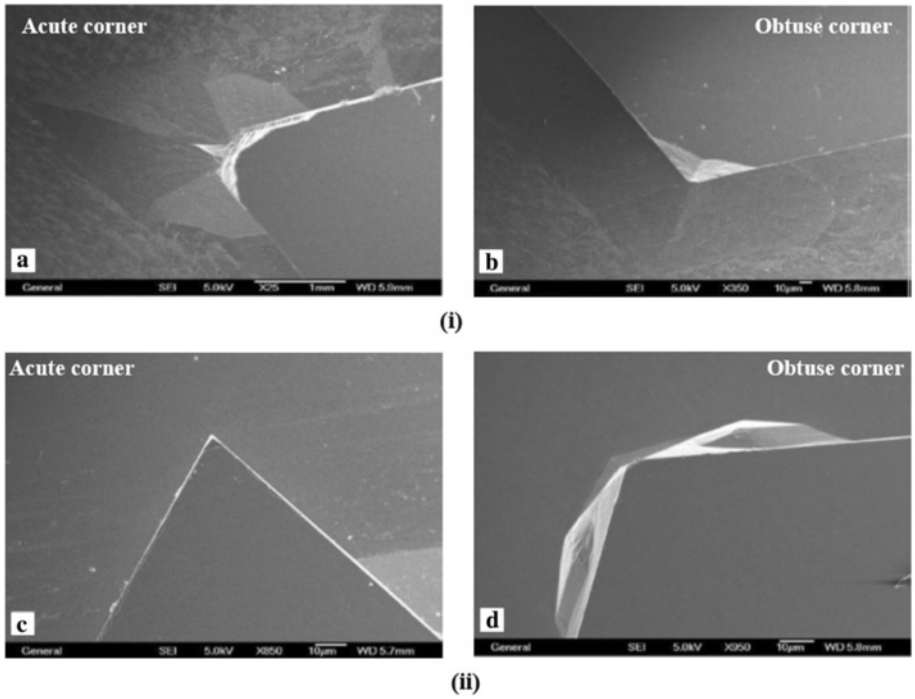

Figure 46 SEM images of convex corners fabricated in (i) pure and (ii) IPA added 40% KOH using rhombus compensation geometry [115]. With permission from Elsevier, Copyright 2006.

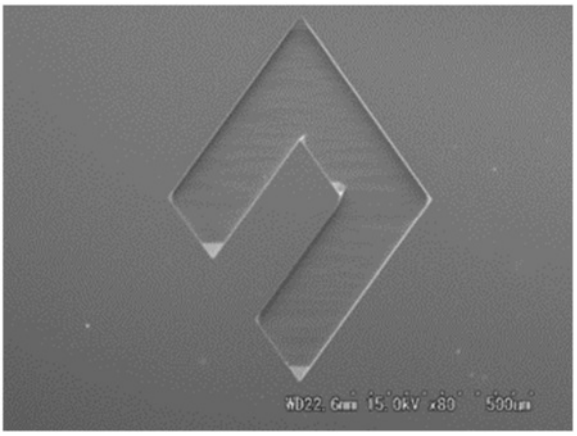

Figure 48 SEM picture of a cantilever beam with vertical sidewalls in {110} wafer realized in 25 wt% TMAH using beam shape compensating pattern at its corners.

uniform photoresist coating, reflection of UV light from tilted sidewalls and the uneven gap between mask and bottom surface. First concern is the uniform coating of photoresist using spin coating method which is most commonly used in microfabrication. Although electrodeposition can be employed to obtain uniform thickness photoresist on uneven surface, it has its own limitations [172-174]. The electrodeposited photoresist needs conductive base on which the photoresist electrodeposition takes place and therefore it cannot be used at all stages of a process. Although the spray coating method provides better results than spinning, it is also not an ideal solution to coat a uniform thickness resist on 3D topography surface such as cavities with a large difference in size on the same sample. The second problem in this method is the reflection of UV light from tilted sidewalls during UV exposure. This unwanted reflection exposes the photoresist of opposite sidewalls. However it can be avoided using polarized UV light, it requires extra hardware in exposure tool [172]. The third issue is the uneven gap between mask and wafer surface. It may cause diffraction problem and can change the feature size transferred from mask to substrate.

(ii) The second method for the fabrication of perfect convex corner also involve two steps of etching and requires two masks [70,112,128,175]. However it does not need any lithography after the first step of etching. Both steps of lithography using photomasks #1 and #2 are employed before the first step of etching. Figure 50 shows the SEM micrographs of the multiple reservoirs connected with each other through V-shaped channels. The convex corners formed by the intersection of the sidewalls are completely protected. The sequence of process steps are illustrated in Figure 51. The fabrication start with the pattering of nitride layer using mask # 1. Afterward, thermal oxidation is performed to grow the oxide layer. This step of oxidation is called local oxidation of silicon (LOCOS) as only exposed silicon is oxidized and remaining part is protected by nitride layer [176]. Now the oxide is patterned for the first step of anisotropic etching (Figure 51(c)). Thereafter, the etching is performed to a required depth (Figure 51(d)). In these structures, it can be noticed that grooves aligned along <110> can be formed in pure TMAH, while those that are aligned with <100> are possible only in surfactant-added TMAH (or IPA added KOH) as the inclusion of surfactant in TMAH (or IPA in KOH) reduces the undercutting at <100> edges. Now, the thermal oxidation is carried out to deposit an oxide layer on exposed silicon (second LOCOS). Again, nitride layer is selectively removed either by dry etching or wet etching in hot phosphoric acid (H_3PO_4). If the nitride is etched out in hot phosphoric acid, sample should be immersed in buffered hydrofluoric acid (BHF) for a short time (about 20 sec) in order to remove any oxide layer formed over the nitride during the LOCOS process [177]. This step is attempted because the oxide etch rate in phosphoric acid is negligible in comparison to nitride etch rate. Subsequently, the buffered oxide is etched out in BHF. Now, the second step of silicon etching is employed. This step of silicon etching should be performed in TMAH as the oxide layer is being used as masking layer. The sidewalls of the currently etched cavities and of the grooves previously formed intersect each other in the shape of the convex corners, which are not etched back as they are passivated by the etch mask. Finally oxide layer is removed in BHF. As shown in SEM picture in Figure 50, the structure fabricated using this method comprise perfect convex corners. However, the process is illustrated for the fabrication of microfluidic channels with multiple reservoirs in Si{100} wafer, it can be utilized for other types of structures which contain convex corners such as proof mass for accelerometer [111]. Moreover this technique can be employed for Si{110} to form the microstructure with perfect convex corner as presented in Figure 52 [128]. Hence this is a generic process. In this method, the overlapped area between two mask is calculated using simple trigonometric relations. Accordingly the dimensions of masks are determined. It may me emphasize here that the dimensions of the mask for the fabrication of microstructure using wet anisotropic etching is determined considering the lateral undercutting and angles of etched sidewalls.

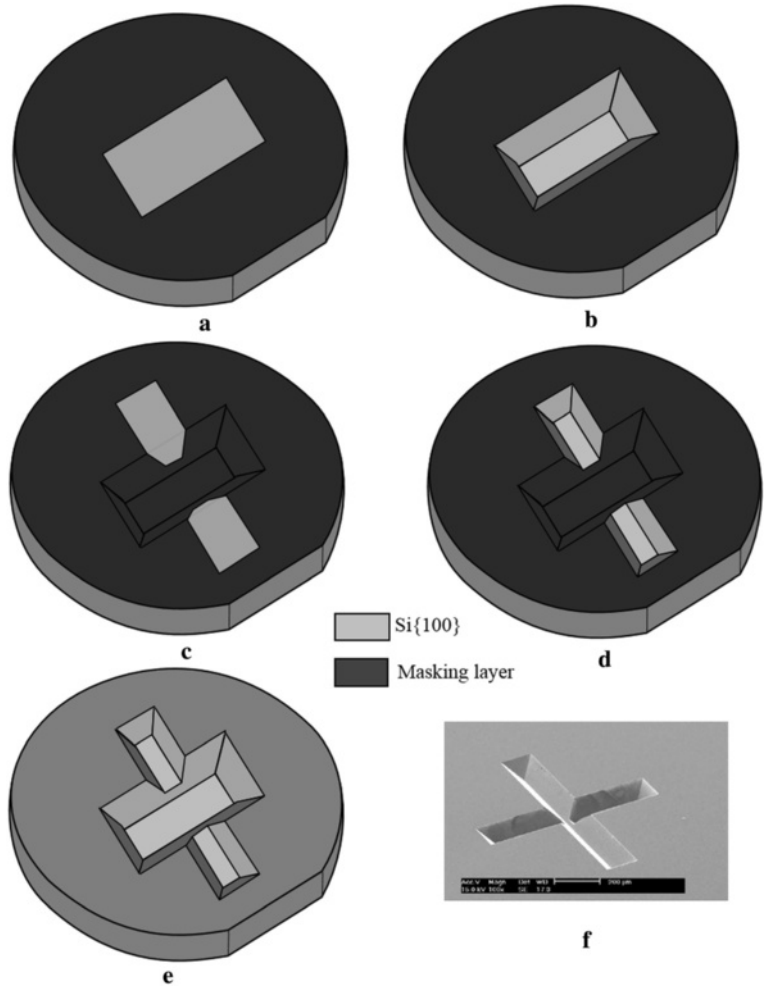

Figure 49 Fabrication sequence for the formation of microstructure with protected convex corners using two-step etching: (a) Deposition and patterning of mask layer; (b) Silicon anisotropic etching; (c) Re-deposition of mask layer followed by patterning (d) Second step of anisotropic etching; (e) Removal of mask layer (f) SEM picture of a structure fabricated using similar process steps (with permission from Elsevier, Copyright 2002) [69].

Conclusions

This topical review is focused on the fabrication methods of convex corners in {100} and {110} oriented silicon wafers using anisotropic wet chemical etching based silicon bulk micromachining. In the corner compensation method, various kinds of compensating geometries used for the formation of protected corners are reviewed and discussed. In this technique, spatial requirement and the resultant shape of etched convex corner are the major concerns. In the case of {100} wafer, <100> oriented compensating design provides sharp edge corner under certain conditions, but its high spatial requirement is a main drawback, especially when the bent grooves are required to be realized. In order to reduce the spatial requirement and to get the sharp convex corner, a compensating geometry designed by superimposed squares is used provided the etchant characteristics fulfill certain requirements. Square shape design needs less space to fit at the corner, but it is not suitable to achieve sharp corners. In the surfactant added TMAH solution, triangular shape design is a best choice. In this etchant, formation of

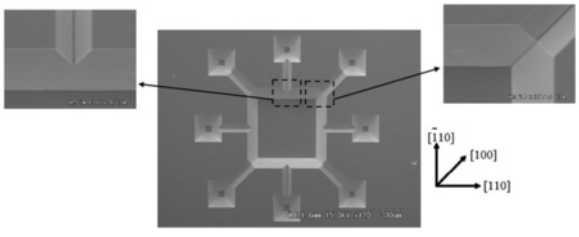

Figure 50 SEM picture of microfluidic channel with multiple reservoirs with perfectly protected corners realized using two-step etching and LOCOS process.

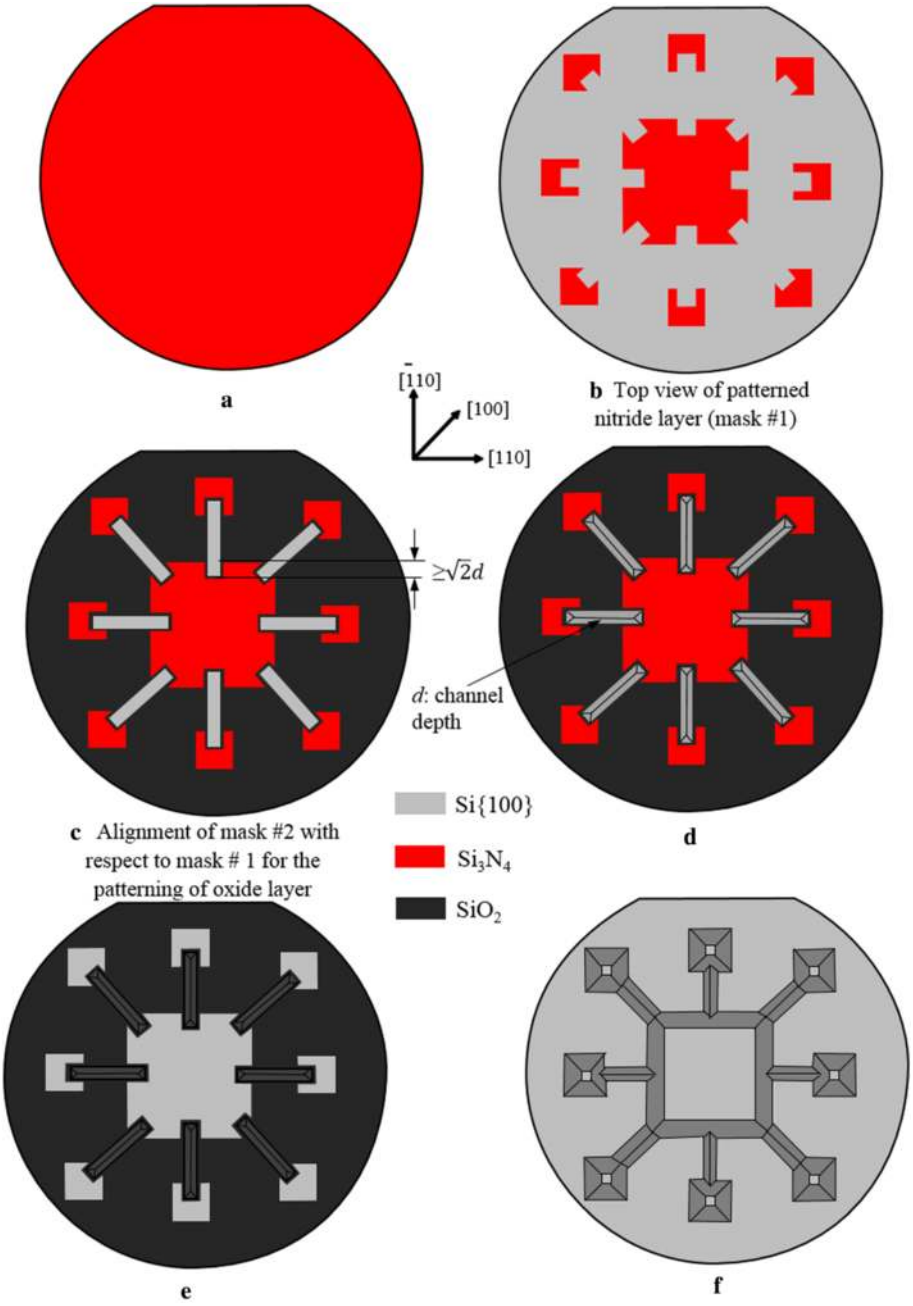

Figure 51 Fabrication steps for the formation of microfluidic channels with multiple reservoirs with perfect convex corners: (a) Si_3N_4 deposited wafer; (b) Patterning of Si_3N_4 layer using mask # 1; (c) Thermal oxidation followed by patterning of oxide layer using mask # 2 (d) Anisotropic etching in surfactant added TMAH (or IPA added KOH) (e) Re-oxidation followed by selective removal of Si_3N_4 (f) Again anisotropic etching in pure TMAH (or KOH) and removal of oxide layer.

bent V-grooves with sharp convex corners is easily achievable. In the corner compensation method, it is concluded that <100> beam is appropriate choice for the formation of sharp convex corner in high concentration TMAH (e.g. 20–25 wt%) and KOH provided space around the convex corner is not a restriction. In the case of spatial restriction, such as bent V-grooves, surfactant added high concentration TMAH with triangular shape compensation geometry is a right choice. In order to protect the convex corner on Si{110} surface, <112> oriented beam (or parallelogramic beam) is an optimal compensating geometry owing to its simple design and the same size beams are used at the acute and obtuse corners.

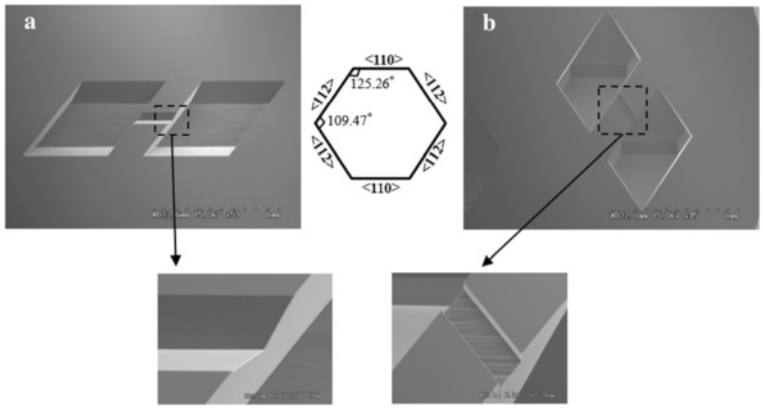

Figure 52 Different shapes of microfluidic channels with multiple reservoirs realized in Si{110} wafer. Microstructures edges are aligned along **(a)** <110> and <112> directions **(b)** <112> directions [128].

Apart from corner compensation methods, two different techniques are also discussed. These methods are very useful when the convex corners with perfectly sharp edges are desired to be fabricated. Unlike the corner compensation method, the formation of sharp convex corner in these methods does not require any time controlled etching. However these techniques provide perfect convex corners, they require two-mask lithography and two-step etching. The extra mask and processing steps make them more expensive and complex.

Competing interests
The authors declare that they have no competing interests.

Authors' contributions
PP carried out literature search and wrote the manuscript. KS reviewed/edited the manuscript. Both authors read and approved the final manuscript.

Authors' information
Dr. Prem Pal did his M.Tech. in Solid State Material (SSM) in December 1999 and Ph.D. in the area of MEMS in December 2004, both from Indian Institute of Technology Delhi (IIT Delhi), India. The *Foundation for Innovation and Technology Transfer (FITT), IIT Delhi* awarded his thesis for "Best Industry Relevant Ph.D. Project −2005". From July 2005 to June 2006, he worked as Postdoctoral Researcher at Yonsei Microsystems Laboratory (YML), School of Mechanical Engineering, Yonsei University Seoul, South Korea. He worked in Sato laboratory, Department of Micro-Nano Systems Engineering, Nagoya University, Nagoya, Japan: from July 2006 to March 2008 as COE Scientist and from March 2008 to March 2010 as JSPS Fellow. He joined the Department of Physics, Indian Institute of Technology Hyderabad in April 2010 as Assistant Professor. Presently, he is working as Associate Professor. He has published more than 40 papers in peer reviewed international journals of high impact factors. His research interests include MEMS technology, MEMS based sensors, Silicon Micromachining, Thin films for MEMS.
Prof. Kazuo Sato graduated from Yokohama National University, Japan and received his BS Degree in 1970. He worked with Hitachi Co. Ltd. in a period of 1970–1994. During this period, he received his PhD degree from the University of Tokyo in 1982. He started Si-micromachining research in 1983 and published 128 international journal papers in MEMS technologies. He joined Nagoya University in 1994 as a full professor at Department of Micro Systems Engineering. He became Emeritus professor of Nagoya University in 2012, and currently is a professor at Aichi Institute of Technology, Japan. His research interests include bulk micromachining of Si and quartz, mechanical characterization of MEMS materials, and MEMS applications. He co-chaired IEEE MEMS-97 conference. He was the editor in Asia (2008–2012) and currently is an editorial board member of the Journal of Micromechanics and Microengineering. He is the founding chair of the Division of Micro/Nano Science and Engineering in the Japan Society of Mechanical Engineers (JSME), and Honorary Member of the JSME. He also is a senior member of IEEJ, and a fellow of JSPE, and a member of IEEE.

Acknowledgments
This work was supported by research grant from the Department of Science and Technology (Project No. SR/S3/MERC/072/2011), New Delhi, India and the Japan Society for the Promotion of Science (JSPS). Sincere thanks to Ms. Michiko Shindo (Secretory to Prof. K. Sato) for her assistance in obtaining permissions to reproduce some figures from published papers and Mr. Sajal Sagar Singh for his suggestions.

Author details
[1]Department of Physics, MEMS and Micro/Nano Systems Laboratory, Indian Institute of Technology Hyderabad, Hyderabad, India. [2]Department of Mechanical Engineering, Aichi Institute of Technology, Toyota, Aichi, Japan.

Received: 23 June 2014 Accepted: 10 January 2015
Published online: 27 May 2015

References
1. Gad-el-Hak M (2002) The MEMS Handbook. CRC Press LLC, Boca Raton
2. Elwenspoek M, Jansen H (1998) Silicon Micromachining. Cambridge University Press, UK
3. Takahata K (2013) Advances in Micro/Nano Electromechanical Systems and Fabrication Technologies. Publisher: InTech.
4. Frühauf J (2005) Shape and functional elements of the bulk silicon microtechnique: a manual of wet-etched silicon structures. Springer.
5. Lindroos V, Tilli M, Lehto A, Motooka T (2010) Handbook of Silicon Based MEMS Materials and Technologies. William Andrew Publishing.
6. Hsu TR (2003) MEMS & Microsystems: Design and Manufacture. Tata McGraw-Hill Publishing Company Ltd, New Delhi, India
7. Madou MJ (2002) Fundamentals of Microfabrication: The Science of Miniaturization, 2nd edn. CRC Press, Boca Raton, US
8. Varadan VK (2006) Smart Material Systems and MEMS: Design and Development Methodologies. John Wiley & Sons Ltd.
9. Bustillo JM, Howe RT, Muller RS (1998) Surface micromachining for microelectromechanical systems. IEEE Proc 86:1552–74
10. Kovacs GT, Maluf NI, Petersen KE (1998) Bulk micromachining of silicon. IEEE Proc 86:1536–1351
11. Petersen KE (1982) Silicon as a mechanical material. IEEE Proc 70:420–457
12. Lang W (1996) Silicon microstructuring technology. Materials Science and Engineering: R: Reports 17:1–55
13. Jansen H, Gardeniers H, Boer MD, Elwenspoek M, Fluitman J (1996) A survey on the reactive ion etching of silicon in microtechnology. J Micromech Microeng 6:14–28

14. Oehrlein GS (1990) Reactive Ion Etching. In: Rossnagel SM, Westwood WD, Haber JJ (eds) Handbook of Plasma Processing Technology-Fundamentals, Etching, Deposition, and Surface Interactions. NJ: Noyes, Park Ridge
15. Coburn JW, Winters HF (1979) Plasma etching-a discussion of mechanisms. J Vac Sci Technol 16:391–403
16. Larmer F, Schilp P (1994) Method of anisotropically etching silicon, German Patent DE 4 241 045.
17. Jiang E, Keating A, Martyniuk M, Prasad K, Faraone L, Jiang JM (2012) Characterization of low-temperature bulk micromachining of silicon using an SF_6/O_2 inductively coupled plasma. J Micromech Microeng 22:095005 (10pp)
18. Hynes AM, Ashraf H, Bhardwaj JK, Hopkins J, Johnston I, Shepherd JN (1999) Recent advances in silicon etching for MEMS using the ASE process. Sens Actuators A 74:13–17
19. Teng J, Prewett PD (2005) Focused ion beam fabrication of thermally actuated bimorph cantilevers. Sens Actuators A 123–124:608–613
20. Walker CK, Narayanan G, Knoepfle H, Capara J, Glenn J, Hungerford A, Bloomstein TM, Palmacci ST, Stern MB, Curtin JE (1997) Laser micromachining of silicon: a new technique for fabricating high quality terahertz waveguide components. In: Proc. 8th International Symposium on Space Terahertz Technology. Harvard University, Cambridge, USA, 25-27 March 1997, p 358. http://www.nrao.edu/meetings/isstt/papers/1997/1997358376.pdf
21. Schwartz B, Robbins H (1976) Chemical etching of silicon. J Electrochem Soc 123(12):1903–1909
22. Zandi K, Arzi E, Izadi N, Mohajerzadeh S, Haji S, Abdi Y, Asl Soleimani E (2006) Study of bulk micromachining for <100> silicon. Eur Phys J Appl Phys 35:7–12
23. Lee DB (1969) Anisotropic etching of silicon. J Appl Phys 40:4569–4575
24. Bean KE (1978) Anisotropic etching of silicon. IEEE Trans Electron Devices ED-25:1185–1193
25. Seidel H, Csepregi L, Heuberger A, Baumgartel H (1990) Anisotropic etching of crystalline silicon in alkaline solutions I: Orientation dependence and behavior of passivation layers. J Electrochem Soc 137(11):3612–3626
26. Seidel H, Csepregi L, Heuberger A, Baumgartel H (1990) Anisotropic etching of crystalline silicon in alkaline solutions II: Influence of Dopants. J Electrochem Soc 137:3626–3632
27. Tabata O, Asahi R, Funabashi H, Shimaoka K, Sugiyama S (1992) Anisotropic etching of silicon in TMAH solutions. Sens Actuators A 34(1):51–57
28. Sato K, Shikida M, Matsushima Y, Yamashiro T, Asaumi K, Iriye Y, Yamamoto M (1998) Characterization of orientation-dependent etching properties of single-crystal silicon: effects of KOH concentration. Sens Actuators A 61:87–93
29. Sato K, Shikida M, Yamashiro T, Tsunekawa M, Ito S (1999) Roughening of single-crystal silicon surface etched by KOH water solution. Sens Actuators A 73:122–130
30. Powell O, Harrison HB (2001) Anisotropic etching of {100} and {110} planes in (100) silicon. J Micromech Microeng 11:217–220
31. Tanaka H, Yamashita S, Abe Y, Shikida M, Sato K (2004) Fast etching of silicon with a smooth surface in high temperature ranges near the boiling point of KOH solution. Sens Actuators A 114:516–520
32. Matsuoka M, Yoshida Y, Moronuki M (1992) Preparation of silicon thin diaphragms free from micropyramids using anisotropic etching in KOH solution. J Chem Eng 25:735–740
33. Baryeka I, Zubel I (1995) Silicon anisotropic etching in KOH-isopropanol etchant. Sens Actuators A 48:229–238
34. Shikida M, Sato K, Tokoro K, Uchikawa D (2000) Differences in anisotropic etching properties of KOH and TMAH solutions. Sens Actuators A 80:179–188
35. Backlund Y, Rosengren L (1992) New shapes in (100) Si using KOH and EDP etches. J Micromech Microeng 27:5–9
36. Sato K, Shikida M, Yamashiro T, Asaumi K, Iriye Y, Yamamoto M (1999) Anisotropic etching rates of single-crystal silicon for TMAH water solution as a function of crystallographic orientation. Sens Actuators A 73:131–137
37. Cheng D, Gosalvez MA, Hori T, Sato K, Shikida M (2006) Improvement in smoothness of anisotropically etched silicon surfaces: Effects of surfactant and TMAH concentrations. Sens Actuators A 125:415–421
38. Pal P, Sato K, Gosalvez MA, Tang B, Hida H, Shikida M (2011) Fabrication of novel microstructures based on orientation dependent adsorption of surfactant molecules in TMAH solution. J Micromech Microeng 21(1):015008, 11pp
39. Pal P, Sato K (2010) Fabrication methods based on wet etching process for the realization of silicon MEMS structures with new shapes. Microsystem Technologies 16(7):1165–1174
40. Gosalvez MA, Tang B, Pal P, Sato K, Kimura Y, Ishibashi K (2009) Orientation and concentration dependent surfactant adsorption on silicon in aqueous alkaline solutions: explaining the changes in the etch rate, roughness and undercutting for MEMS applications. J Micromech Microeng 19(12):125011, 18pp
41. Yan G, Chan Philip CH, Hsing IM, Sharma RK, Sin JKO, Wang Y (2001) An improved TMAH Si-etching solution without attacking exposed aluminum. Sens Actuators A 89:135–141
42. Chen PH, Peng HY, Hsieh CM, Chyu MK (2001) The characteristic behavior of TMAH water solution for anisotropic etching on both Silicon substrate and SiO_2 layer. Sens Actuators A 93(2):132–137
43. Tellier CR, Charbonnieras AR (2003) Characterization of the anisotropic chemical attack of (hhl) silicon plates in a TMAH 25 wt% solution: micromachining and adequacy of the dissolution slowness surface. Sens Actuators A 105:62–75
44. Zhang J, Hon WC, Leung LLW, Chen KJ (2005) CMOS-compatible micromachining techniques for fabricating high-performance edge-suspended RF/microwave passive components on silicon substrates. J Micromech Microeng 15:328–335
45. Steinsland E, Finstad T, Hanneborg A (2000) Etch rates of (100), (111), and (110) single-crystal silicon in TMAH measured in situ by laser reflectance interferometry. Sens Actuators A 86:73–80
46. Wu MP, Wu QH, Ko WH (1986) A study on deep etching of silicon using ethylenediamine-pyrocatechol-water. Sens Actuators A 9:333–343
47. Reisman A, Berkenblit M, Chan SA, Kaufmann FB, Green DC (1979) The controlled etching of silicon in catalyzed ethylene-diamine-pyrochatechol-water solutions. J Electrochem Soc: Solid-State Sci Technol 126:1406–15
48. Kern W (1978) Chemical etching of silicon, germanium, gallium arsenide, and gallium phosphide. RCA Review 39:278–307
49. Declercq MJ, Gerzberg L, Meindl JD (1975) Optimization of the hidrazine-water solution for anisotropic etching of silicon in integrated circuit technology. J Electrochem Soc: Solid State Science 122:545–552
50. Schnakenberg U, Benecke W, Lochel B (1990) NH_4OH-based etchant for silicon micromachining. Sens Actuators A 23:1031–1035
51. Clarck LD Jr, Lund JL, Edell DJ (1988) Cesium hydroxide (CsOH): A useful etchant for micromachining silicon. In: Tech. Digest, IEEE Solid State Sensor and Actuator Workshop (Hilton Head Island, SC, 6-9 June 1988) pp 5–8. http://ieeexplore.ieee.org/xpl/articleDetails.jsp?arnumber=26419
52. Robertson SV, Katehi LPB, Rebeiz GM (1996) Micromachined w-band filters. IEEE Transactions on Microwave Theory and Techniques 44:598–606
53. Blondy P, Brown AR, Cros D, Rebeiz GM (1998) Low loss micromachined filters for millimeter-wave communication systems. IEEE Trans Microwave Theory Tech 46:2308–2316
54. Papapolymerou I, Drayton RF, Katehi LPB (1998) Micromachined patch antennas. IEEE Transactions on Antennas and Propagation 46:275–83
55. Rebeiz G M (2003) RF MEMS: Theory, Design, and Technology. John Wiley & Sons Inc.
56. Burrer C, Esteve J, Lora-Tamayo E (1996) Resonant silicon accelerometers in bulk micromachining technology-An approach. J Microelectromech Syst 5:122–130
57. Yu JC, Lan CB (2001) System modelling of microaccelerometer using piezoelectric thin films. Sens Actuators A 88:178–186
58. Wur DR, Davidson JL, Kang WP, Kinser DL (1995) Polycrystalline diamond pressure sensor. J Microelectromech Syst 4:34–41
59. Wang CC, Gogoi BP, Monk DJ, Mastrangelo CH (2000) Contamination-insensitive differential capacitive pressure sensors. J Microelectromech Syst 9:538–543
60. Bae B, Flachsbart BR, Park K, Shannon MA (2004) Design optimization of a piezoresistive pressure sensor considering the output signal-to-noise ratio. J Micromech Microeng 14:1597–1607
61. Yang H, Bao M, Yin H, Shen S (2002) A novel bulk micromachined gyroscope based on a rectangular beam-mass structure. Sens Actuators A 96:145–151
62. Van Herwaarden AW, Van Duyn DC, Van Oudheusden BW, Sarro PM (1989) Integrated thermopile sensors. Sens Actuators A 22:621–630
63. Sarro PM, van Hexwaarden AW, van der Vlist W (1994) A silicon-silicon nitride membrane fabrication process for smart thermal sensors. Sens Actuators A 41–42:666–671
64. Dillner U, Kessler E, Poser S, Baier V, Mtiller J (1997) Low power consumption thermal gas-flow sensor based on thermopiles of highly effective thermoelectric materials. Sens Actuators A 60:1–4
65. Olson EA, Efremov MY, Zhang M, Zhang Z, Allen LH (2003) The design and operation of a MEMS differential scanning nanocalorimeter for high-speed

heat capacity measurements of ultrathin films. J Microelectromech Syst 12:355–364
66. Winter W, Hohne GWH (2003) Chip-calorimeter for small samples. Thermochimica Acta 403:43–53
67. Zhang Y, Tadigadapa S (2004) Calorimetric biosensors with integrated microfluidic channels. Biosensors and Bioelectronics 19:1733–1743
68. Koch M, Schabmueller CGJ, Evans AGR, Brunnschweiler A (1999) Micromachined chemical reaction system. Sens Actuators A 74:207–210
69. Kwon JW, Kim ES (2002) Multi-level microfluidic channel routing with protected convex corners. Sens Actuators A 97–98:729–733
70. Pal P, Sato K (2009) Various shapes of silicon freestanding microfluidic channels and microstructures in one step lithography. J Micromech Microeng 19(5):055003 (11pp)
71. Kwon JW, Yu H, Kim ES (2005) Film transfer and bonding techniques for covering single-chip ejector array with microchannels and reservoirs. J Microelectromech Syst 14(6):1399–1408
72. Vashist SK (2007) A review of microcantilevers for sensing applications. AZoJono – Journal of. Nanotechnology 3:1–15
73. Wee KW, Kang GY, Park J, Kang JY, Yoon DS, Parkb JH, Kim TS (2005) Novel electrical detection of label-free disease marker proteins using piezoresistive self-sensing micro-cantilevers. Biosensors and Bioelectronics 20:1932–1938
74. Lee JH, Hwang KS, Park J, Yoon KH, Yoon DS, Kim TS (2005) Immunoassay of prostate-specific antigen (PSA) using resonant frequency shift of piezoelectric nanomechanical microcantilever. Biosensors and Bioelectronics 20:2157–62
75. Battiston FM, Ramseyer JP, Lang HP, Baller MK, Gerber C, Gimzewski JK, Meyer E, Guntherodt HJ (2001) A chemical sensor based on a microfabricated cantilever array with simultaneous resonance frequency and bending readout. Sens Actuators B 77:122–131
76. Neuzil P, Nagarajan R (2006) The formation of sharp AFM tips by single step etching. J Micromech Microeng 16:1298–1300
77. Burt DP, Dobson PS, Donaldson L, Weaver JMR (2008) A simple method for high yield fabrication of sharp silicon tips. Microelectronic Engineering 85:625–630
78. Han J, Lu S, Li Q, Li X, Wang J (2009) Anisotropic wet etching silicon tips of small opening angle in KOH solution with the additions of I2/KI. Sens Actuators A 152:75–79
79. Pal P, Singh SS (2013) A new model for the etching characteristics of corners formed by Si{111} planes on Si{110} wafer surface. Engineering 5(11):1–8
80. Trieu HK, Mokwa W (1998) A generalized model describing corner undercutting by the experimental analysis of TMAH/IPA. J Micromech Microeng 8:80–83
81. Chahoud M, Wehmann HH, Schlachetzki A (1998) Etching simulation of convex and mixed InP and Si structures. Sens Actuators A 69:251–258
82. Schroder H, Obermeier E (2000) A new model for Si{100} convex corner undercutting in anisotropic KOH etching. J Micromech Microeng 10:163–170
83. Shikida M, Nanbara K, Koizumi T, Sasaki H, Sato K, Odagaki M, Ando M, Furuta S, Asaumi K (2000) A Model explaining mask-corner undercut phenomena in anisotropic silicon etching: a saddle point in the etching-rate diagram. Sens Actuators A 97–98:758–63
84. Chang Chien WT, Chang CO, Lo YC, Li ZW, Chou CS (2005) On the Miller-indices determination of Si{100} convex corner undercut planes. J Micromech Microeng 15:833–842
85. Merlos A, Acero MC, Bao MH, Bausells J, Esteve J (1992) A study of the undercutting characteristics in the TMAH:IPA system. J Micromech Microeng 2:181–183
86. Dong W, Zhang X, Liu C, Li M, Xu B, Chen W (2004) Mechanism for convex corner undercutting of (110) silicon in KOH. Microelectronics J 35:417–419
87. Pal P, Singh SS (2013) A simple and robust model to explain convex corner undercutting in wet bulk micromachining. Micro and Nano Systems Letters 1(1):1–6
88. Bean KE, Runyan WR (1977) Dielectric isolation: comprehensive, current and future. J Electrochem Soc 124:5C–12C
89. Abu-Zeid M (1984) Corner undercutting in anisotropically etched isolation contours. J Electrochem Soc 131:2138–2142
90. Wu XP, Ko WH (1989) Compensating corner undercutting in anisotropic etching of (100) silicon. Sens Actuators A 18:207–215
91. Puers B, Sansen W (1990) Compensation structures for convex corner micromachining in silicon. Sens Actuators A 23:1036–1041
92. Mayer GK, Offereins HL, Sandmaier H, Kuhl K (1990) Fabrication of non-underetched convex corners in anisotropic etching of (100) silicon in aqueous KOH with respect to novel micromechanic elements. J Electrochem Soc 137:3947–3951
93. Offereins HL, Kühl K, Sandmaier H (1991) Methods for the fabrication of convex corners in anisotropic etching of (100) silicon in aqueous KOH. Sens Actuators A 25:9–13
94. Sandmaier H, Offereins HL, Kuhl K, Lang W (1991) Corner compensation techniques in anisotropic etching of (100)-silicon using aqueous KOH. In: 6th International Conference on Solid State Sensors and Actuators (Transducers 91, San Francisco, CA, 24-27 June 1991) pp 456–459. http://ieeexplore.ieee.org/xpl/login.jsp?tp=&arnumber=148910&url=http%3A%2F%2Fieeexplore.ieee.org%2Fiel2%2F505%2F3940%2F00148910.pdf%3Farnumber%3D148910
95. Hui WC (1991) Technique for protecting chip corners in wet chemical etching of silicon wafers. Technical Report Lawrence Livermore National Lab, CA (United States)
96. Offereins HL, Sandmaier H, Marusczyk K, Kuhl K, Plettner A (1992) Compensating corner undercutting of (100) silicon in KOH. Sensors and Materials 3:127–144
97. Bao M, Chr B, Esteve J, Bausells J, Marco S (1993) Etching front control of <110> strips for corner compensation. Sens Actuators A 37–38:727–732
98. Scheibe C, Obermeier E (1995) Compensating corner undercutting in anisotropic etching of (100) silicon for chip separation. J Micromech Microeng 5:109–111
99. Kampen RP, Wolffenbuttel RF (1995) Effects of <110>−oriented corner compensation structures on membrane quality and convex corner integrity in (100)-silicon using aqueous KOH. J Micromech Microeng 5:91–94
100. Zhang Q, Liu L, Li Z (1996) A new approach to convex corner compensation for anisotropic etching of (100) Si in KOH. Sens Actuators A 56:251–254
101. Enoksson P (1997) New structure for corner compensation in anisotropic KOH etching. J Micromech Microeng 7:141–144
102. Chung CK, Lee CC, Wu CY (1998) A novel approach to corner compensation of multistep Si(100) terraced structure for microlens. IEEE/LEOS summer topical meeting, Monterey, CA
103. Long M K, Burdick J W, Antonsson E K (1999) Design of compensation structures for anisotropic etching. In: Technical Proceedings of the 1999 International Conference on Modeling and Simulation of Microsystems (MSM 99).
104. Ma L (2001) Robust mask-layout and process synthesis in micro-electro-mechanical-systems (MEMS) using genetic algorithms. Ph.D. Thesis California Institute of Technology Pasadena, California
105. Tellier C (2003) CAD design of mask compensation patterns. Proc IEEE Sensors 1:517–522
106. Wacogne B, Sadani Z, Gharbi T (2004) Compensation structures for V-grooves connected to square apertures in KOH-etched (100) silicon: theory, simulation and experimentation. Sens Actuators A 112:328–339
107. Fan W, Zhang D (2006) A simple approach to convex corner compensation in anisotropic KOH etching on a (100) silicon wafer. J Micromech Microeng 16:1951–1957
108. Mukhiya R, Bagolini A, Margesin B, Zen M, Kal S (2006) <100>bar corner compensation for CMOS compatible anisotropic TMAH etching. J Micromech Microeng 16:2458–2462
109. Pal P, Sato K, Chandra S (2007) Fabrication techniques of convex corners in a (100)-silicon wafer using bulk micromachining: a review. J Micromech Microeng 17:R1–R23
110. Biswas K, Das S, Kal S (2006) Analysis and prevention of convex corner undercutting in bulk micromachined silicon microstructures. Microelectronics J 37:765–769
111. Pal P, Chandra S (2004) Recessed microstructures with perfect convex corners for accelerometers. Sensor Letters 2:226–231
112. Pal P, Chandra S (2004) A novel process for perfect convex corner realization in bulk micromachining. J Micromech Microeng 14:1416–1420
113. Kawakatsu H, Saya D, Kato A, Fukushima K, Toshiyoshi H, Fujita H (2002) Millions of cantilevers for atomic force microscopy. Review of Scientific Instruments 73(3):1188–1192
114. Chu HY, Fang W (2004) A vertical convex corner compensation and non {111} crystal planes protection for wet anisotropic bulk micromachining process. J Micromech Microeng 14:806–813
115. Jia C, Dong W, Liu C, Zhang X, Zhou J, Zhong Z, Xue H, Zang H, Xu B, Chen W (2006) Convex corners undercutting and rhombus compensation

in KOH with and without IPA solution on (110) silicon. Microelectronics J 37:1297–1301
116. Kim B, Cho DD (1998) Aqueous KOH etching of silicon (110) etch characteristics and compensation methods for convex corners. J Electrochem Soc 145:2499–508
117. Ciarlo DR (1987) Corner compensation structures for (110)-oriented silicon. Proc. IEEE Micro Robots and Teleoperators Workshop, Hyannis, MA, USA
118. Wacogne B, Zeggari R, Sadani Z, Gharbi T (2006) A very simple compensation technique for bent V-grooves in KOH etched (100) silicon when thin structures or deep etching are required. Sens Actuators A 126:264–269
119. Kummamuru RK, Hu L, Cook L, Efremov MY, Olson EA, Allen LH (2008) A close proximity self-aligned shadow mask for sputter deposition onto a membrane or cavity. J Micromech Microeng 18:095027 (9pp)
120. Pal P, Sato K, Shikida M, Gosalvez MA (2009) Study of corner compensating structures and fabrication of various shapes of MEMS structures in pure and surfactant added TMAH. Sens Actuators A 154:192–203
121. Yu JC (2011) Convex comer compensation for a compact seismic mass with high aspect ratio using anisotropic wet etching of (100) silicon. In: Symposium on Design, Test, Integration and Packaging of MEMS/MOEMS (DTIP-11, Aix-en-Provence, France, 11-13 May, 2011) pp 197–199. http://ieeexplore.ieee.org/xpl/login.jsp?tp=&arnumber=6107993&url=http%3A%2F%2Fieeexplore.ieee.org%2Fiel5%2F6095278%2F6107967%2F06107993.pdf%3Farnumber%3D6107993
122. Mukhiya R, Bagolini A, Bhattacharya TK, Lorenzelli L, Zen M (2011) Experimental study and analysis of corner compensation structures for CMOS compatible bulk micromachining using 25wt% TMAH. Microelectronics J 42:127–134
123. Bagolini A, Faes A, Decarli M (2010) Influence of etching potential on convex corner anisotropic etching in TMAH solution. J Microelectromech Syst 19(5):1254–1259
124. Smiljanic MM, Jovic V, Lazic Z (2012) Maskless convex corner compensation technique on a (100) silicon substrate in a 25 wt% TMAH water solution. J Micromech Microeng 22:115011 (11pp)
125. Shayan M, Arezoo B, Vanini AS, Kotamjani AA (2011) Silicon (100) undercutting modelling and corner compensation structures design in wet anisotropic etching process. Proc. IMechE Part B: J. Engineering Manufacture 225:1041–1049. http://pib.sagepub.com/content/225/7/1041.abstract
126. Apanius M, Kaul B, Abramsona AR (2007) Silicon shadow mask fabrication for patterned metal deposition with microscale dimensions using a novel corner compensation scheme. Sens Actuators A 140:168–175
127. Giousouf M, Assmus F, Kuck H (1999) Structuring of convex corners using a reoxidation process-application to a tuning fork resonator made from (110)-silicon. Sensors and Actuators A 76:416–424
128. Pal P, Gosalvez MA, Sato K, Hida H, Xing Y (2014) Anisotropic etching on Si{110}: Experiment and simulation for the formation of microstructures with convex corners. J Micromech Microeng 24:125001 (25pp)
129. Cho WJ, Chin WK, Kuo CT (2004) Effects of alcoholic moderators on anisotropic etching of silicon in aqueous potassium hydroxide solutions. Sens Actuators A 116:357–368
130. Zubel I, Kramkowska M (2004) Etch rates and morphology of silicon (hkl) surfaces etched in KOH and KOH saturated with isopropanol solutions. Sens Actuators A 115:549–556
131. Philipsen HGG, Kelly JJ (2009) Influence of chemical additives on the surface reactivity of Si in KOH solution. Electrochimica Acta 54:3526–3531
132. Zubel I, Kramkowska M (2001) The effect of isopropyl alcohol on etching rate and roughness of (100) Si surface etched in KOH and TMAH solutions. Sensors and Actuators A 93:138-147. http://www.sciencedirect.com/science/article/pii/S0924424701006483
133. Zubel I, Kramkowska M (2002) The effect of alcohol additives on etching characteristics in KOH solutions. Sens Actuators A 101:255–261
134. Pal P, Gosalvez MA, Sato K (2010) Silicon micromachining based on surfactant-added tetramethyl ammonium hydroxide: etching mechanism and advanced application. Japan J Appl Phys 49:056702 (9pp)
135. Gosalvez MA, Pal P, Tang B, Sato K (2010) Atomistic mechanism for the macroscopic effects induced by small additions of surfactants to alkaline etching solutions. Sens Actuators A 157:91–95
136. Tang B, Pal P, Gosalvez MA, Shikida M, Sato K, Amakawa H, Itoh S (2009) Ellipsometry study of the adsorbed surfactant thickness on Si{110} and Si{100} and the effect of pre-adsorbed surfactant layer on etching characteristics in TMAH. Sens Actuators A 156:334–341
137. Pal P, Sato K, Gosalvez MA, Kimura Y, Ishibashi K, Niwano M, Hida H, Tang B, Itoh S (2009) Surfactant adsorption on single crystal silicon surfaces in TMAH solution: orientation-dependent adsorption detected by in-situ infra-red spectroscopy. J Microelectromech Syst 18:1345–1356
138. Yang CR, Chen PY, Yang CH, Chiou YC, Lee RT (2005) Effects of various ion-typed surfactants on silicon anisotropic etching properties in KOH and TMAH solutions. Sens Actuators A 119:271–281
139. Yang CR, Yang CH, Chen PY (2005) Study on anisotropic silicon etching characteristics in various surfactant-added tetramethyl ammonium hydroxide water solutions. J Micromech Microeng 15:2028–2037
140. Sato K, Uchikawa D, Shikida M (2001) Change in orientation-dependent etching properties of single-crystal silicon caused by a surfactant added to TMAH solution. Sens Mater 13:285–291
141. Sarro PM, Brida D, van der Vlist W, Brida S (2000) Effect of surfactant on surface quality of silicon microstructures etched in saturated TMAHW solutions. Sensors Actuators A 85:340–345
142. Sekimura M (1999) Anisotropic etching of surfactant-added TMAH solution. In: Proc. 12th IEEE International Conference on Micro Electro Mechanical Systems. (MEMS-99 Orlando, Florida, 17-21 Jan. 1999) pp 650–655. http://ieeexplore.ieee.org/xpl/login.jsp?tp=&arnumber=746904&url=http%3A%2F%2Fieeexplore.ieee.org%2Fxpls%2Fabs_all.jsp%3Farnumber%3D746904
143. Yang CR, Chen PY, Chiou YC, Lee RT (2005) Effects of mechanical agitation and surfactant additive on silicon anisotropic etching in alkaline KOH solution. Sens Actuators A 119:263–270
144. Resnik D, Vrtacnik D, Aljancic U, Mozek M, Amon S (2005) The role of Triton surfactant in anisotropic etching of {110} reflective planes on (100) silicon. J Micromech Microeng 15:1174–1183
145. Xu YW, Michael A, Kwok CY (2011) Formation of ultra-smooth 45° micromirror on (100) silicon with low concentration TMAH and surfactant: Techniques for enlarging the truly 45° portion. Sens Actuators A 166:164–71
146. Pal P, Sato K, Gosalvez MA, Shikida M (2007) Study of rounded concave and sharp edge convex corners undercutting in CMOS compatible anisotropic etchants. J Micromech Microeng 17:2299–2307
147. Zubel I, Kramkowska M, Rola K (2012) Silicon anisotropic etching in TMAH solutions containing alcohol and surfactant additives. Sens Actuators A 178:126–135
148. Rola KP, Zubel I (2013) Triton surfactant as an additive to KOH silicon etchant. J Microelectromech Syst 22:1373–1382
149. Tanaka H, Umeki N, Sato K (2013) Perfect adsorption of ppb-level surfactant in 5% KOH water solution on a silicon surface changing anisotropic etching properties. In: 17th International Conference on Solid-State Sensors, Actuators and Microsystems (Transducers & Eurosensors XXVII, Barcelona, Spain, 16-20 June 2013) pp 1978–1981. http://ieeexplore.ieee.org/xpl/articleDetails.jsp?arnumber=6627183
150. Wind RA, Hines MA (2000) Macroscopic etch anisotropies and microscopic reaction mechanisms: a micromachined structure for the rapid assay of etchant anisotropy. Surface Science 460:21–38
151. Wind RA, Jones H, Little MJ, Hines MA (2002) Orientation-resolved chemical kinetics: using microfabrication to unravel the complicated chemistry of KOH/Si etching. J Phys Chem B 106:1557–1569
152. Gosalvez MA, Pal P, Ferrando N, Hida H, Sato K (2011) Experimental procurement of the complete 3D etch rate distribution of Si in anisotropic etchants based on vertically micromachined wagon wheel samples. J Micromech Microeng 21:125007 (14pp)
153. Gosalvez MA, Pal P, Ferrando N, Sato K (2011) Reliability assessment of the complete 3D etch rate distribution of Si in anisotropic etchants based on vertically micromachined wagon wheel samples. J Micromech Microeng 21:125008 (12pp)
154. Gosalvez MA, Pal P, Sato K (2011) Reconstructing the 3D etch rate distribution of silicon in anisotropic etchants using data from vicinal {100}, {110} and {111} surfaces. J Micromech Microeng 21:105018 (17pp)
155. James TD, Parish G, Winchester KJ, Musca CA (2006) A crystallographic alignment method in silicon for deep, long microchannel fabrication. J Micromech Microeng 16:2177–2182
156. Chang WH, Huang YC (2005) A new pre-etching pattern to determine <110> crystallographic orientation on both (100) and (110) silicon wafers. Microsystem technologies 11:117–128
157. Ensell G (1996) Alignment of mask pattern to crystal orientations. Sens Actuators A 53:345–8

158. Vangbo M, Bäcklund Y (1996) Precise mask alignment to the crystallographic orientation of the silicon wafers using wet anisotropic etching. J Micromech Microeng 6:279–284
159. Lai JM, Chieng WH, Huang YC (1998) Precision alignment of mask etching with respect to crystal orientation. J Micromech Microeng 8:327–329
160. Tseng FG, Chang KC (2003) Precise [100] crystal orientations determinations on <110>−orientated silicon wafers. J Micromech Microeng 13:47–52
161. Pal P, Chandra S (2004) Bulk-micromachined structures inside anisotropically etched cavities. Smart Mater Struct 13:1424–1429
162. Chandra S, Singh J, Chand A (1997) Design and development of microstructures for MEMS applications. Proc SPIE 3226:22–30
163. Abedinov N, Grabiec P, Gotszalk T, Ivanov TZ, Voigt J, Rangelow IW (2001) Micromachined piezoresistive cantilever array with integrated resistive microheater for calorimetry and mass detection. J Vac Sci Technol A 19:2884–2888
164. Gosalvez MA (2003) Atomistic modeling of anisotropic etching of crystalline silicon. PhD Thesis, Dissertation 123, Dissertations of Laboratory of Physics, Helsinki University of Technology.
165. Jaccodine RJ (1962) Use of modified free energy theorems to predict equilibrium growing and etching shapes. J Appl Phys 33:2643–2647
166. Pal P, Haldar S, Singh SS, Ashok A, Xing Y, Sato K (2014) A detailed investigation and explanation to the appearance of different undercut profiles in KOH and TMAH. J Micromech Microeng 24:095026 (9pp)
167. Kutchoukow VG, Mollinger JR, Bossche A (1999) Novel method for spinning of photoresist on wafers with through-hole. In: Proc. 13th European Conf. on Solid-State Transducers (Eurosensors) pp 256–72
168. Craven D (1996) Photolithography challenges for micromachining industry, Proc. SPIE 2884, 16th Annual BACUS Symposium on Photomask Technology and Management, 498 (Dec. 27, 1996) pp 1–10. http://spie.org/Publications/Proceedings/Paper/10.1117/12.262838
169. Venstra WJ, Spronck JW, Sarro PM, Eijk JV (2009) Photolithography on bulk micromachined substrates. J Micromech Microeng 19:055005 (6pp)
170. Luxbacher T, Mirza A (1999) Spray coating for MEMS, interconnects, and advanced packaging applications. Sensors 16:61–64
171. Singh VK, Sasaki M, Hane K, Esashi M (2004) Flow condition in resist spray coating and patterning performance for three-dimensional photolithography over deep structures. Japan J Appl Phys 43:2387–2391
172. Linder S, Baltes H, Gnaedinger F, Doering E (1996) Photolithography in anisotropically etched grooves. In: Proc. 9th Annual International Workshop on Micro Electro Mechanical Systems (MEMS-96, 11-15 Feb 1996) pp 38-43. http://ieeexplore.ieee.org/xpl/login.jsp?tp=&arnumber=493826&url=http%3A%2F%2Fieeexplore.ieee.org%2Fxpls%2Fabs_all.jsp%3Farnumber%3D493826
173. Kersten P, Bouwstra S, Petersen JW (1995) Photolithography on micromachined 3-D surfaces using electrodeposited photoresist. Sens Actuators A 51:51–54
174. Heschel M, Bouwstra S (1998) Conformal coating by photoresist of sharp corners of anisotropically etched through-holes in silicon. Sens Actuators A 70:75–80
175. Pal P, Sato K (2009) Complex three dimensional structures in Si{100} using wet bulk micromachining. J Micromech Microeng 19:105008 (9pp)
176. Appels JA, Kooi E, Paffen MM, Schatorje JJH, Verkuylen WHCG (1970) Local oxidation of silicon and its application in semiconductor devices Technology. Philips Res Repts 25:118–132
177. Loewenstein LM, Tipton CM (1991) Chemical etching of thermally oxidized silicon nitride: comparison of wet and dry etching methods. J Electrochem Soc 138:1389–1394